RSC Advances

ROYAL SOCIETY OF CHEMISTRY

www.rsc.org/advances

Anisotropic ion transport in nanostructured solid polymer electrolytes

Shan Cheng, [a§] *Derrick M. Smith,* [a§] *Qiwei Pan,* [a, b] *Shijun Wang,*[a] *and Christopher Y. Li* [a*]

[a] Department of Materials Science and Engineering, Drexel University, Philadelphia, PA 19104, USA

[b] Department of Materials Science and Engineering, South China University of Technology, Guangzhou 510640, China

*Corresponding author, C.Y. Li (Email: chrisli@drexel.edu. Tel: 215-895-2083. Fax: 215-895-6760)

[§] equal contribution.

Abstract: Solid polymer electrolytes (SPEs) with good room temperature ionic conductivity and a high shear modulus are needed for future energy storage devices. Extensive study has been devoted to searching for SPE with these desired properties. In this review, we will discuss recent progresses on the correlation between nanoscale morphology and ion conductivity in SPEs. Specifically, we will focus on anisotropic ion transport in five different types of SPEs with distinct morphological controls: crystalline structure, block copolymers, mechanical stretching, hybrids/nanocomposites, and holographic polymerization.

Introduction

Lithium-ion batteries are the system of choice for portable electronic devices and they dominate our consumer market today.[1-13] The term lithium ion battery represents a family of secondary (rechargeable) devices where both electrodes are intercalation materials, and the electrolyte is a lithium salt dissolved in a mixture of organic solvents. The advantages of a lithium-ion battery include high energy density, flexible and light weight design, and long lifespan. Even higher power densities can be achieved if lithium metal is used as the anode instead of a lithium intercalation material to form a lithium metal battery, and this high power density is particularly critical for applications such as electric cars. Lithium metal batteries were first fabricated back in 1972; in spite of the impeccable operation of the cathode, the system was proven not viable because the formation of Li dendrites at the Li/liquid electrolyte interface during charge-discharge processes could lead to explosion hazards. In order to circumvent this problem, the Li metal anode was replaced with intercalation materials, which led to the current lithium-ion batteries commercialized by Sony Corporation. However, this material swap for stability was at the expense of sacrificing power density, and there are still safety-related issues with these lithium–ion batteries as well. To prevent lithium dendrite growth, an alternative approach is to use solid polymer electrolytes (SPEs) to form lithium polymer batteries (LPB): it has been found that lithium dendrite formation and the explosion hazard associated with it can be avoided if the shear modulus of the SPE is sufficiently high.[1, 2, 6, 9, 11, 12 13]

The development of SPEs began in the 1970s — shortly after Wright *et al.* reported the semicrystalline structure of complexes between polyethylene oxide (PEO) and alkali salts in 1973[14] and the following study on its electrical properties.[15, 16] It was then proposed to use these polymer-alkali salt complexes as solid electrolytes for high energy density battery applications since they combine solid-state electrochemistry with the advantage of naturally versatile and easy processing of plastics. Since then, interests in this emerging area spanned worldwide. Early investigations focused on understanding the correlation between morphology and conductivity of these complexes. It was initially speculated that ions are transported through the polymer helices in the crystalline phase, similar to inorganic ion conductors, while later studies demonstrated that only the amorphous phase accounts for ion conduction.[17-20] The linkage between polymer segmental dynamics and ion transport in the early 1980s largely determined the trend of SPE research: tremendous efforts were devoted to inhibiting polymer crystallization. The strategies that have been developed include modification of the polymer structure with different architectures, such as comb-like polymers with short chain PEO or cross-linked network polymers.[21-24] However, the major issue with these approaches is that reducing the crystallinity of the polymer would inevitably sacrifice the mechanical properties of the material, which contradicts the original intention of using mechanically robust polymer membranes for safer battery applications. To find a balance between fast ion transport and high mechanical property, several approaches were developed during the mid to late 1980s, including polymer blends SPEs, block copolymer SPEs, and ceramic reinforced SPEs.[25-28] Development of single ion polymer conductors started in the mid 1980s in recognition of the importance of high cation transference number for battery performance.

The last two decades witnessed a class of nanocomposite SPEs developed by Scrosati *et al.*, and it appears to be an interesting group of candidates for high performance lithium battery applications due to their enhanced mechanical, thermal, electrochemical stability, and room temperature conductivity.[29-31] The discovery of fast ion transport in some $P(EO)_6LiX$ crystalline complexes led to a reconsideration of the fundamental ion conduction mechanism in polymer electrolytes.[32-34] Decoupling of ionic conductivity from polymer segmental relaxation has recently been proposed, which provides a novel concept for new SPE designs.[35, 36] With the aid of computer modeling, the polymer dynamics and ion association in both polymer/salt blends and single ion conductors have been studied systematically.[37-44] Figure 1 is a general summary of the development of various SPE systems during the last four decades.

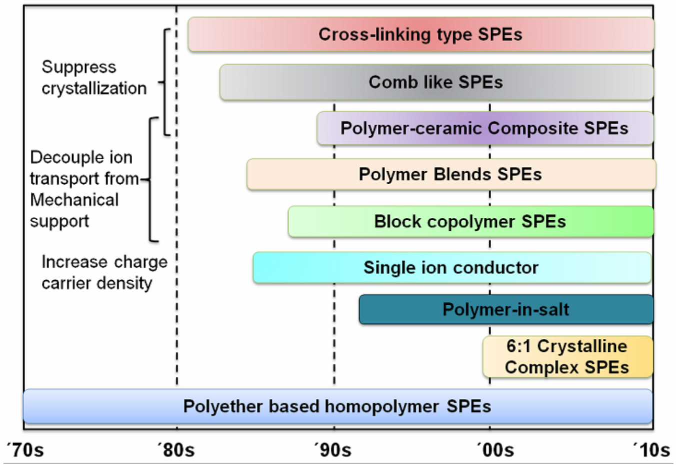

Figure 1. Summary of solid polymer electrolyte development during the last four decades.

A number of excellent reviews have been published recently discussing various types of SPE for electrochemical device applications.[1-13, 25-28] In this article, we will discuss the correlation between SPE morphology and ion transport. Specifically, we will focus on anisotropic ion transport according to morphological anisotropy. We will first discuss ion transport in polymers, followed by five different types of morphological controls in SPE: crystalline structure, block copolymers, mechanically induced orientation, hybrids/nanocomposites, and holographic polymerization.

2. Ion transport in SPE

In general, there are three types of mechanisms governing ionic charge transport. First, in liquid electrolytes, solvent molecules are mobile and can form complexes with the ions, and the entire complex traverse together under external fields. Second, in solids such as β-alumina, ions reside in potential wells. Sufficient activation can induce displacement of bare ions while the other components of the lattices are strictly immobile. Third, in polymer electrolytes, since polymer chains are entangled, it's more difficult for the complexed chains to physically transport "long distance" with the associated ions as they would in a liquid system; however, above the glass transition temperature, significant chain segmental motion exists, which enables a solvation-desolvation process along the chain. When chain segmental motion allows substitution of the anion site for an additional neighboring ligand, the charged pairs are separated and move in opposite directions. To this end, in order to effectively solvate the salt and form polymer-lithium complex, the following basic criteria need to be satisfied for the host polymers: (i) a high dielectric constant (ε); (ii) high electron-donor characteristics, usually found in polymers with a high concentration of sequential polar groups on their backbone, such as ether (–O–), sulfide (–S–), amine (–N–), phosphine (–P–), carbonyl (C=O) and cyano (C≡N), which are good candidates for complex formation;[22, 45] (iii) appropriate distance between coordinating centers, which is best illustrated by crown ethers;[46, 47] (iv) a flexible backbone and low steric hindrance for bond rotation; (v) easy to synthesize and process. PEO is one of the most extensively studied polymers for SPE because it exhibits superior ability to form complexes with a variety of metal salts.[24, 45, 48-50] The ethylene oxide unit (CH_2CH_2O) has strong electron donating capability and an optimal heteroatom spacing; both characteristics facilitate the dissociation of the salt. The high flexibility of the PEO chain, indicated by a low glass transition temperature, allows for reorganization of the chain for cation coordination. Polypropylene oxide (PPO) is another candidate as an ion-hosting polymer. Although it remains amorphous at room temperature favoring ion mobility, the solvation ability is less effective than PEO due to its low dielectric constant and steric hindrance imposed by the additional methyl groups.[45, 48] Other polymers, such as polysiloxanes, poly(ethylene succinate) and poly(ethylene imine), have shown a certain capacity for complex formation with alkali metal salts, but are far less studied than PEO–based polyethers.[45, 48]

Only salts with a low lattice energy have been demonstrated to form complexes with a given polymer host.[45] These salts are usually characteristic of large anions with negative charges well dispersed by the electron withdrawing ligands. The higher the degree of charge delocalization, the better the solvation of the salt is in a given host. The dissociation constant for commonly used anions follows the order below[48, 49, 51, 52]:

$(CF_3SO_2)_2N^-$, $AsF_6^- > PF_6^- > ClO_4^- > BF_4^- > CF_3SO_3^- > CF_3CO_2^-$

Other factors that need to be taken into consideration for the salt to be used as solute in the electrolyte include: high solubility and conductivity, inert against electrodes, wide electrochemical window, good thermal stability, and minimum toxicity. Summaries on the property and performance of different types of salts can be found in several reviews.[25, 51, 53]

As previously mentioned, one of the greatest challenges for SPE development is to improve the room temperature conductivity to at least 10^{-4} S/cm while maintaining the shear modulus of the electrolyte sufficiently high (~ 7GPa suggested by computational simulation[54]) to inhibit lithium dendrite formation. During the last few decades, tremendous efforts have been made to develop novel SPE systems that can meet the desired performance requirement; these strategies generally fall into the following three scenarios: (i) Designing of a multiphase SPE to decouple ion transport from the mechanical support; (ii) Improving conductivity anisotropy, optimizing ion conducting pathways by creating directional and continuous conducting channels; (iii) Developing single ion conductors to increase charge carrier density. Table 1 summarizes the properties of a number of selected SPEs recently reported. The following sections will provide detailed discussions with the focus on anisotropic ion transport.

Table 1. Selective examples of current SPE systems.

Type of SPE	**Category**	**Examples**	**σ (S/cm) @ T(°C)**	**Mechanical strength (Pa)**	**Ref**
BCP SPE	(i)	PS-P(S-g-EO)-PS+LiTFSI (O/Li=20)	$2\text{x}10^{-5}$ @ RT	10^{8} *(1)*	55
		PSt-*b*-PPME-*b*-PSt (80% PEO content)	~10^{-4} @ RT	$5\text{x}10^{6}$	56
		PS-*b*-PEO+LiTFSI (O/Li=50)	~10^{-3} @ 90	~10^{8} @ 90 *(2)*	57
LC-BCP SPE	(i), (ii)	PEO-*b*-PMA/CB+$LiClO_4$ (O/Li=120)	$2\text{x}10^{-7}$ @ 20 *(3)*	N/A	58
		2/$LiCF_3SO_3$	$1.5\text{x}10^{-6}$ @ 35 *(4)*	N/A	59
PEO-ceramic nanofiller	(i), (iii)	PEG(M_n 250 Da)/LiTFSI (O/Li=20) + 20wt% fumed silica	10^{-3} @ RT	10^{5} @ RT	60
		$P(EO)_8LiClO_4$ + 10wt% TiO_2 (13nm)	$1.75\text{x}10^{-5}$ @ RT	N/A	29
Stretched SPE	(ii)	$P(EO)_7LiI$	~10^{-4} @ RT *(5)*	N/A	61
HP	(i), (ii)	Norland 65+ PEG(400 Da)+LiTFSI (O/Li=19) @ 45 v/v %	$1.93\text{x}10^{-5}$ @ RT	N/A	62
Single ion conductor	(iii)	PCHFEM-Li/PEO (M_w 400 kDa) blend	~10^{-5} @ 100	N/A	63
		P(MEO-MALi)	$2\text{x}10^{-7}$ @ RT	N/A	64
		P(STFSILi)-*b*-PEO-*b*-P(STFSILi) @ O/Li=27	~10^{-5} @ 60	~$9\text{x}10^{6}$ *(6)*	65

Note: BCP: Block copolymer, LC: Liquid Crystalline
(1): Dynamic Young's modulus was measured at 1 Hz.

(2): Shear modulus was measured using parallel plate rheometer.
(3): Ionic conductivity was measured parallel to PEO cylinder long axis.
(4): Ionic conductivity was measured parallel to the smectic layer.
(5): d.c. conductivity was measured along the stretching direction using four-probe-electrode setup.
(6): Tensile strength was measured at 40°C on a DMA at 0.1N/min ramp force.

3. Crystalline morphology directed ion transport

3.1 Phase diagrams of PEO based SPE

It is helpful to start our discussion with a phase diagram of a SPE. Taking PEO as an example, the phase behavior and crystalline morphology of PEO-lithium salts SPEs have been extensively studied since 1980s.[19, 20, 66-72] Several phases are defined in a PEO-lithium salt SPE: a crystalline PEO phase, amorphous PEO-lithium complex phase, and stoichiometric crystalline PEO-lithium complex phases. The number and types of phases depend on the anions, salt concentration and thermal history, and can be determined by X-ray diffraction, NMR, thermal analysis or polarized light microscopy (PLM).[66] We define three regions of semicrystalline SPE based on the type of phases present in the electrolyte at room temperature. Dilute electrolytes (typically at an O/Li molar ratio less than 20) consist of two phases: a crystalline PEO phase and an amorphous PEO-lithium complex phase. Semi-dilute electrolytes (an O/Li molar ratio of approximately 8-20) have the most complicated morphology where multiple phases co-exist, including crystalline PEO, an amorphous PEO-lithium complex phase and a crystalline PEO-lithium complex phase. A concentrated SPE (or polymer in salt) consists of crystalline complexes with stoichiometry of 6:1, 4:1, 3:1 or 2:1 depending on the type of anion. Semi-dilute and concentrated regions are of practical importance since that is where the optimal ionic conductivity is often observed.

Figure 2 shows the reported phase diagrams of a few commonly studied PEO-lithium salt SPEs.[66, 73] Stoichiometric compounds of 6:1 and 3:1 are found in the SPEs containing $LiClO_4$, $LiAsF_6$ and $LiN(CF_3SO_2)_2$ (LiTFSI), while only a PEO-lithium 3:1 complex is identified in PEO-$LiCF_3SO_3$ SPEs. A eutectic point with a melting temperature of 50 - 55 °C is observed for all types of SPEs at a composition range ~ 10 < O/Li molar ratio < 100 except for low M_w PEO-LiTFSI SPE, in which a crystallinity gap between 6 < O/Li < 12 is observed due to the plasticizing effect of the anion. $P(EO)_6LiAsF_6$ has a melting temperature of 136 °C, which is 70 °C higher than that of $P(EO)_6LiClO_4$. Most $P(EO)_3LiX$ complexes have melting temperatures above 100 °C.

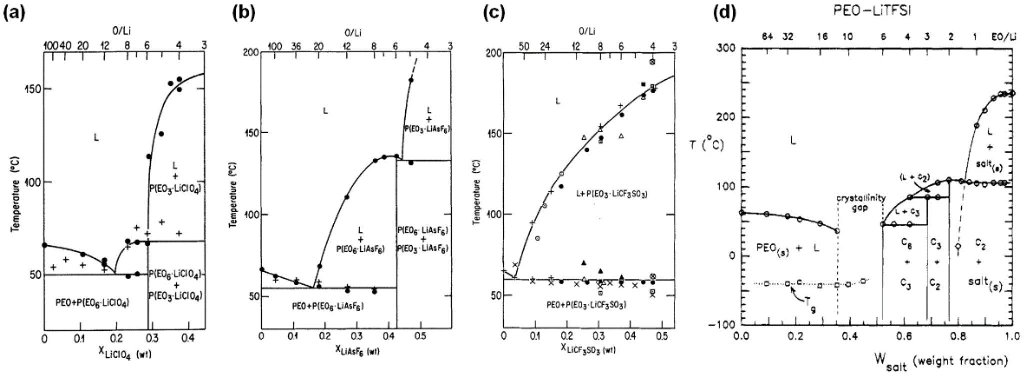

Figure 2. Phase diagrams of a series PEO-LiX electrolytes: (a) PEO-$LiClO_4$; (b) PEO-$LiAsF_6$; (c) PEO-$LiCF_3SO_3$; (d) PEO-LiTFSI. (a-c) are reprinted with permission from *J. Electrochem. Soc.*, 133(2): 315-325 (1986). Copyright 1986, The Electrochemical Society; (d) is reprinted with permission from *Macromolecules*, 1994, 27, 7469-7477. Copyright (1994) American Chemical Society.

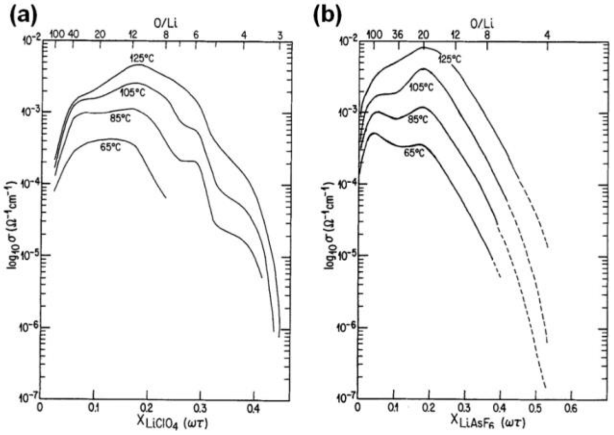

Figure 3. Ionic conductivity as a function of salt content at various temperatures for (a) PEO-$LiClO_4$ system; (b) PEO-$LiAsF_6$ system. Reprinted with permission from *J. Electrochem. Soc.*, 133(2): 315-325 (1986). Copyright 1986, The Electrochemical Society.

The ionic conductivity, σ, can be correlated to the concentration of free ions, or ions contributing to charge flow, p¸ and the diffusion coefficient, D, with the Nernst-Einstein relationship, Eq. (1):

$$\sigma = \frac{pq^2D}{k_BT}, \qquad (1)$$

The overall conductivity of the polymer electrolytes is determined by (i) the number of charge carriers; (ii) degree of charge dissociation, and (iii) the interaction between the ions and the polymer chain, all of which are strongly affected by the ion concentration. For most of the SPE systems above the PEO melting temperature, the optimized ionic conductivity is achieved at an O/Li molar ratio of 8~ 20, as shown in Figure 3. In the dilute region, the ionic conductivity increases monotonically with ion concentration due to the increased number of charge carriers. Above the optimal concentration, ionic conductivity begins to decrease as a result of significant ion pairing and physical cross-linking between polymer chain and Li^+, and from the formation of PEO-Li crystalline complex that restricts the ion mobility. At temperatures below T_m, the concentration dependence on ionic conductivity is complicated by PEO crystallization.

3.2 Ion conduction in crystalline SPE complex

At high concentrations, PEO forms stoichiometric crystalline compounds with Li^+ cations. These crystalline compounds are generally believed to be insulating except for certain $P(EO)_6$:$LiXF_6$ crystalline complexes (X= P, As, Sb) that were reported by Bruce *et al.*[32, 74, 75] The structure of this 6:1 crystalline electrolyte was resolved from powder diffraction data; one example ($P(EO)_6$:$LiAsF_6$ crystalline complex) is shown in Figure 4a.[32, 74-76] The crystalline complex adopts a monoclinic unit cell with two PEO chains interlocking to form cylinders with Li^+ cations residing in a row inside each of the cylinders. Each PEO chain adopts a non-helix conformation of $ctg\bar{g}tgc\bar{g}tcttgt\bar{g}cgt$. The anions are located between the cylinders and do not coordinate with Li^+. The crystalline structures of all three complexes are similar, and the Li^+ coordination number and Li-O bond strength remain unchanged for all three crystalline complexes. As the anion size increases from PF_6^- to AsF_6^- to SbF_6^-, the volume of the unit cell expands by pushing the cylinders apart along *b* and *c* axis and stretching the polymer chain along *a* axis.

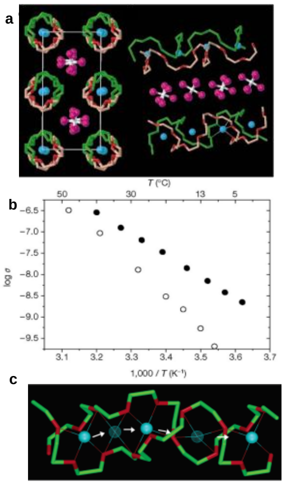

Figure 4. (a) Crystal structure of $P(EO)_6$:$LiAsF_6$ crystalline complex; (b) Temperature dependent ionic conductivity of crystalline (solid circle) and amorphous (open circle) P(EO)6:$LiSbF_6$; (c) Schematic illustration of Li+ diffusion pathways in a $P(EO)_6LiPF_6$ crystalline complex. Figure 4(a) and (b) are reprinted by permission from Macmillan Publishers Ltd: *Nature*, 2001, 412, 520-

523, copyright (2001). Figure 4(c) is reprinted with permission from *J. Am. Chem. Soc.*, 2003, 125, 4619-4626. Copyright (2003) American Chemical Society.

The temperature dependent ionic conductivity of crystalline $P(EO)_6$:$LiSbF_6$ as shown in Figure 4b suggests that ion conduction not only takes place in crystalline phases, but also is faster compared with that in more mobile amorphous phases. The conductivity plot of $P(EO)_6$:$LiSbF_6$ exhibits typical Arrhenius behavior, indicating an ion hopping mechanism is dominating for the ion conduction. The Li^+ diffusion pathway within the cylinder is also proposed based on the crystal structure and is illustrated in Figure 4c. The migration of Li^+ from one site to the neighboring site is facilitated by the presence of vacancy defects.

Despite that promising ion conduction has been demonstrated in these $P(EO)_6$:$LiXF_6$ crystalline complexes, the room temperature conductivities (10^{-7}~10^{-8} S/cm) are still not sufficient for lithium battery applications. Substituting $LiXF_6$ with a salt-bearing large delocalized anion, such as $TFSI^-$, improves the conductivity by one to two orders of magnitude due to the disruption of the potential around Li^+ in the region of $TFSI^-$ anion.[34] Increasing the PEO polydispersity or replacing the methoxy capped chain end with $–OC_2H_5$ group may further improve the conductivity by one order of magnitude via introducing more defects that lead to an increased concentration of charge carriers.[78] Another limitation for using these crystalline SPE is that the optimal ionic conductivity is at M_w of 1000 Da, relatively small for practical applications; further increasing the M_w significantly reduces ion conductivity due to the increase of grain boundaries and misalignment of the crystallites that impedes ion transport.

3.3 Ion conduction in semi-crystalline SPE

As previously discussed, the crystallization of linear PEO has been long viewed as unfavorable for ion conduction. PLM experiments reveals that PEO crystallizes into fringed spherulites in dilute SPE, due to the strong interference with lithium salts.[79-81] During the PEO crystallization process, lithium salts are expelled from the crystals and enrich the amorphous phase between adjacent spherulites, as well as in the amorphous inter-lamellar region. The inhomogeneity of the SPE can be probed using impedance spectroscopy.[82] In semi-dilute electrolytes, both the PEO-lithium complex (salt-rich) and the PEO (salt-poor) phases crystallize into spherulitic morphology.[67, 69] The salt-rich crystalline complexes also exhibit a regularly and densely packed spherulitic morphology but with higher melting temperatures.[19, 20, 83] In addition to inter-spherulite boundaries, individual spherulites are comprised of crystalline lamellae and amorphous regions, with typical thickness of a few nm. This rather complex morphology certainly affects macroscopic conductivity of the corresponding SPE, and in many cases, leads to conductivity anisotropy.

Generally speaking, the impact of crystallization can be categorized into three aspects: (i) decreasing the effective fraction of amorphous conducting phase; (ii) restricting chain mobility (dynamic/tethered chain effect) and (iii) introducing tortuous pathways for ion transport (tortuosity effect). Although extensive studies have been conducted to understand the correlation between crystallization and ionic conductivity reduction, obtaining quantitative analysis is challenging since those three factors are usually intertwined. The temperature dependent conductivity plots of semicrystalline PEO SPEs provide some useful information on the degree of conductivity reduction due to PEO crystallization. Figure 5 shows the conductivity plots of a series of $P(EO)_nLiClO_4$ electrolytes. A conductivity “knee” is observed for electrolytes at all concentrations around the PEO melting temperature, T_m (~60 to 70 °C), below which the conductivity quickly drops to below 10^{-7} S/cm. This 2-3 orders of magnitude of conductivity reduction at room temperature results from the decrease of the conducting phase volume fraction, restriction of chain mobility, and the increased tortuosity as mentioned earlier, whereas the contributions from each factor cannot be quantitatively deconvoluted. All SPEs follow a typical Arrhenius behavior below the T_m of PEO, suggesting that the long range polymer segmental motion is restricted and ion hopping is the major ion conducting mechanism. The steeper slopes at low temperatures indicates that there is a higher energy barrier for ion transport in semicrystalline SPEs.

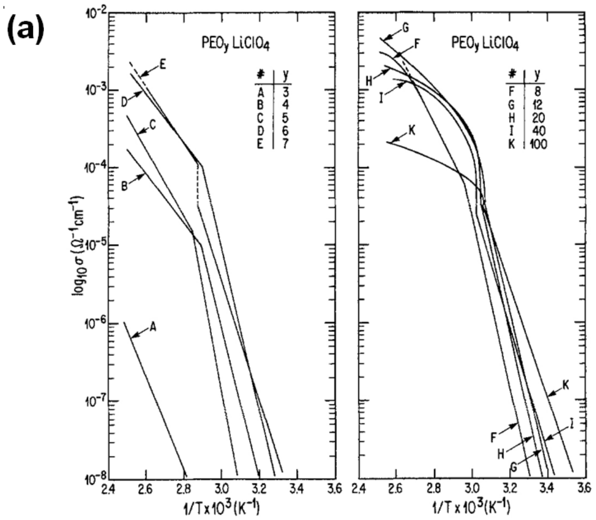

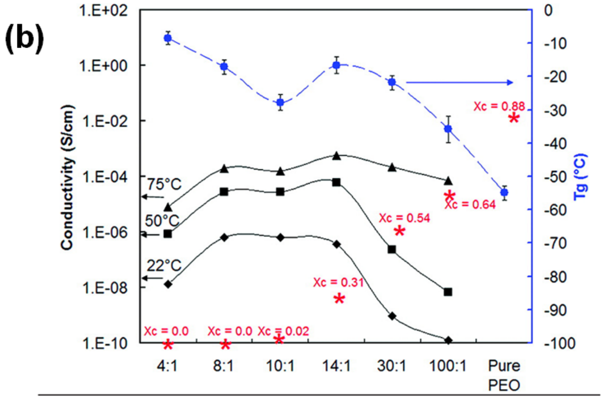

overall EO:Li	X_c (%)	T_g (°C)	effective EO:Li
8:1	0	−17	8:1
10:1	2	−28	10:1
14:1	31	−16.5	8:1

Figure 5. (a) Temperature dependent ionic conductivity for solution cast $P(EO)_nLiClO_4$ electrolytes, reprinted with permission from *J. Electrochem. Soc.*, 133(2): 315-325 (1986). Copyright 1986, The Electrochemical Society (b) Ionic conductivities, glass transition temperatures (T_g) and crystallinity (*) as a function of $LiClO_4$ concentration at different temperatures for PEO-$LiClO_4$ SPE, adapted with permission from *Macromolecules*, 2009, 42, 2142-2156. Copyright (2009) American Chemical Society.

Although the highest ionic conductivity is expected to be in the completely amorphous state where the chain mobility is higher, an interesting observation has been reported by Fullerton-Shirey *et al.* on solution cast PEO-$LiClO_4$ SPE systems.[84] The plot in Figure 5b shows that the 14:1 (O/Li molar ratio) sample with 31% crystallinity has comparable and even higher ionic conductivity than the 8:1 sample that is completely amorphous at 22 °C and 50 °C, respectively, though the effective Li^+ concentration (normalized by PEO crystallinity) and the T_g of the two SPE are the same. Apparently in this case, the ion conduction is decoupled from chain mobility and the enhanced ionic conductivity in semicrystalline SPE indicates that there might be a faster ion transport in the amorphous conducting phase when confined by the PEO crystalline lamellae.

3.4 Ion conduction in polymer single crystal SPE

We recently demonstrated that in addition to the well-known slowed dynamics of the tethered amorphous chain, the tortuous ion diffusion pathway associated with 2D polymer lamellar crystals is critical to the overall observed conductivity reduction. We quantitatively deconvoluted these two factors by preparing a model system (a SPE comprised of polymer single crystals and lithium salts, noted as polymer single crystal SPE) with precisely controlled crystalline morphology and crystal orientation.[85] Polymer single crystals have been used for a variety of applications, and polymer single crystal SPEs are one of the most recent developments.[86-103] To prepare the SPEs with precisely controlled morphology, PEO single crystals were first grown in dilute pentyl acetate solution using a self-seeding method.[86-90] Because of the well-controlled crystallization conditions, the obtained PEO single crystals have a uniform size: they are approximately ~ 20 × 20 μm wide (Figure 6a) and ~ 10 nm thick, and therefore can be viewed as quasi-2D nanoplates. The single crystal suspension was slowly casted onto a PTFE substrate and dried under vacuum at room temperature to yield a single crystal film with an average thickness of ~ 20 μm (Figure 6c). 2D WAXD experiments were conducted with the X-ray beam parallel to the film surface, and the in-plane diffraction pattern reveals well oriented patterns with (120) equatorial diffractions at $2\theta = 19.15°$ and (032) diffraction at $2\theta = 23.3°$ in the quadrants. Detailed analysis of the pattern shows that the polymer chains are aligned parallel to the film's normal and the Herman's orientation factor of (120) diffraction, f_{120}, is calculated to be 0.80. The period of the lamellar stacks is 9.6 nm, which is comprised of two layers of amorphous loops attached to the crystalline stems. The crystallinity X_c is estimated to be 0.77 based on the integrations of isotropic WAXD patterns. Combining SAXS and WAXD results, the thickness of each amorphous loop layer is calculated to be approximately 1.1 nm, and the crystalline stems have a thickness of 7.4 nm.

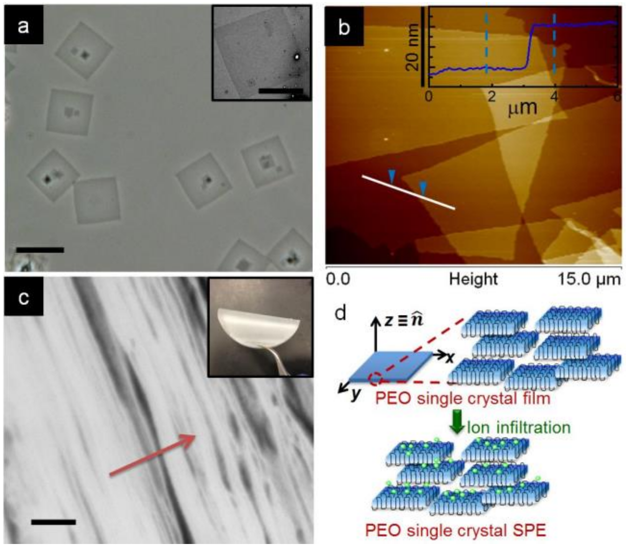

Figure 6. (a) Phase contrast optical microscopy image of PEO single crystals grown from dilute solution before casting into films (scale bar is 20 μm). Inset shows a transmission electron micrograph of a typical single crystal (scale bar is 10 μm); (b) Atomic force microscopy height image of a 15 x 15 μm area scan of PEO single crystals. Inset shows the corresponding height profile along the white line; (c) Scanning electron micrograph of the cross-section of a PEO single crystal film, red arrow shows the film normal (scale bar is 200 nm). Inset shows the optical image of the dry film; (d) Schematic of PEO single crystal SPE preparation.[85] Reprinted with permission from *Macromolecules*, 2014, 47, 3978-3986. Copyright (2014) American Chemical Society.

To prepare PEO single crystal SPEs, $LiClO_4$ was infiltrated into the above mentioned PEO single crystal films by soaking the latter in a $LiClO_4$ / pentyl acetate solution at various salt concentrations and infiltrating times. To simplify the system, we controlled the Li^+ concentration in the region of $0.001 < r < 0.05$, where r is the molar ration between Li^+ and EO group, so that only crystalline PEO and amorphous PEO–Li complex are present. SAXS and WAXD show that we can adopt a 2-phase model with a PEO crystalline phase and an amorphous PEO/Li^+ salt phase to analyze the ion transport behavior: all the ions are confined in a 2D space with a thickness of ~ 2–3 nm. We then used an effective Li^+ to EO molar ratio by normalizing r with the corresponding crystallinity of each SPE, denoting the normalized r as $<r>$ ($<r> = r/(1-Xc)$). Figure 7 shows that both in-plane conductivity $\sigma_{//}$ and through-plane conductivity $\sigma_{\perp}$ increase rapidly with <r> at low Li^+ ion concentrations (<r> < 0.02), and nearly plateau when <r> > 0.02. The conductivity difference along these two directions can be quantified by defining an anisotropy factor as $A = \sigma_{//}/\sigma_{\perp}$. For <$r$> < 0.02, A is approximately 800-2000, and it decreases to 100–300 when <r> > 0.02. A modified Nielsen's model, which is typically used to describe the relative permeability in polymer nanocomposites containing platelet–like nanofillers, was used to explain the conductivity anisotropy:[104-106]

$$R_\mathrm{p} = \frac{1-\phi_\mathrm{s}}{1+\frac{L}{2W}\phi_\mathrm{s}\left(\frac{2}{3}\right)\left(S+\frac{1}{2}\right)} = R_\sigma \qquad (2)$$

Where R_p is the relative permeability of the nanocomposite compared with pristine polymer, ϕ_s is the volume fraction of the filler, L/W is the aspect ratio of the filler, and S is order parameter of the filler and is defined as $S = \frac{1}{2}\langle 3\cos^2\theta - 1\rangle$, where θ is the angle between the platelet normal and the diffusion direction. If we treat the crystalline portion of the 2D PEO single crystals as platelet-like nanofillers and the amorphous fold regions as the matrix, equation (2) can be used to describe the relative permeability of lithium ions (R_σ) diffusing through the single crystal SPE compared to an amorphous matrix. The anisotropy factor $A = \sigma_{//}/\sigma_{\perp} = R_{\sigma//}/R_{\sigma\perp}$ was calculated to be 668 at $\phi_\mathrm{s} = 0.77$, and 521 at $\phi_\mathrm{s} = 0.6$. The calculated value fits well with the measured anisotropy at the lower r region and is slightly higher than the measured value at the higher r region. This discrepancy may be because Nielsen's model is usually used to describe non-interacting gas molecules diffusing through a composite system and is only valid when the molecule size is much smaller than the nanofiller dimension.

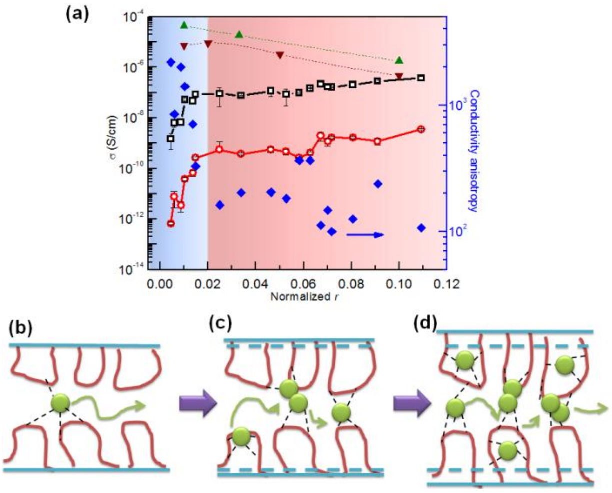

Figure 7. (a) Ionic conductivity and conductivity anisotropy at RT as a function of normalized *r*. (black open square – $\sigma_{//}$ of single crystal SPE; red open circle – $\sigma_{\perp}$ of single crystal SPE; blue solid diamond – conductivity anisotropy $\sigma_{//}/\sigma_{\perp}$ of single crystal SPE; green triangle – σ_0 of linear PEO-$LiClO_4$ SPE; brown inverted triangle – σ_0 of network PEO-$LiClO_4$ SPE from *ref*[107]) (b-d) shows that ions are confined in the PEO fold regions at different concentration.[85] Reprinted with permission from *Macromolecules*, 2014, 47, 3978-3986. Copyright (2014) American Chemical Society.

Figure 7 also shows the differences between $\sigma_{//}$ and isotropic amorphous SPE at corresponding ion contents (σ_0). At $r = 0.1$, σ_0 can be directly measured immediately after quenching the SPE from 120°C to room temperature because the SPE remains 100% amorphous due to the slow crystallization kinetics at this ion concentration. A Vogel-Tamman-Fulcher (VTF) equation was used to fit the high temperature (above melting) data and extrapolate the plot to room temperature,[108-110] shown as the green triangles in Figure 7. As a comparison, σ_0 of cross-linked PEO network (100% amorphous) SPE reported by Watanabe *et al.* [107] are also shown in Figure 7. Despite a slight discrepancy of the σ_0 values, which is likely due to cross-linking effects, the conductivities for both linear amorphous and network SPEs gradually decrease with increasing Li^+ concentration, due to the increase of glass transition. In the dilute ion region, *e.g.* <*r*> = 0.01 and the effective EO to Li ratio is 100:1, there are ~ 12 loops per Li^+

on the crystal surface. Considering Li^+ ions are confined between two fold surfaces, each Li^+ ion has to hop over ~ 2-3 loops, or approximately ~1 nm, to reach another ion as depicted in Figure 7b. It would be more difficult energetically for these tethered segments to adjust their local conformation in order to assist the multiple hopping of each ion compared with amorphous SPE. At higher salt concentrations, $\langle r \rangle = 0.11$ for example, there is approximately one Li^+ ion per loop, allowing Li^+ to efficiently hop among PEO loops. The tethered chain effect seems to be overwhelmed by the cross-linking introduced by the Li^+ ions themselves, and the only effect of crystallization on the overall conductivity of SPE is tortuosity. Furthermore, the molecular conformation of the loop and the typically crosslinked amorphous PEO are likely different. The loops are well defined and locally pinned between the adjacent crystalline stems, while the linear amorphous PEO, even crosslinked, may undergo long or semi-long range reptation.

3.5 Summary of crystalline structure effect on ion transport

In summary, the ion conduction in linear PEO based SPEs is complicated by crystallization. Although there is a direct correlation between polymer dynamics and ion transport in most of these SPEs, cautions need to be taken when interpreting the ionic conductivity in a specific SPE system. The segmental motion alone cannot fully explain the ion conduction phenomenon in crystalline SPE. The nanoscale structure and morphology of the electrolytes are also important factors that contribute to the overall ionic conductivity.

4. Anisotropic ion transport in Block copolymer SPE

4.1 Phase behavior and ion distribution in BCP SPE

Due to the unique micro-phase separated structure, block copolymer SPEs containing rigid reinforcing segment and soft ion conducting segment provide an elegant solution for decoupling of mechanical properties and ionic conductivity.[27, 56, 57, 111-119] The degree of phase separation of the block copolymer is governed by the Flory-Huggins interaction parameter (χ). Depending on the degree of polymerization (N) and the volume fraction (f) of each block, the morphology of a linear AB diblock copolymer could change from spherical (S), cylindrical (C), gyroid (G), and lamellar (L) [120, 121]. The most commonly studied block copolymer SPE are based on polymer/salt blends in which the salt is preferentially dissolved in the PEO block. Introduction of lithium salt into the conducting domain significantly influences the phase behavior of the block copolymer and ultimately impacts the ionic conductivity of the SPE.[57, 111, 122-133] The shift in phase behaviors in these block copolymer SPE systems is attributed to the change of Flory-Huggins interaction parameter (χ) due to the introduction of the salt. The complexation between PEO chains and lithium ions typically results in an increased incompatibility between the PEO domain and the non-conducting domain, driving the phase separation towards the strong segregation region. On the other hand, this ordered nanostructure renders property anisotropy of block copolymer SPE.

Ion distribution in block copolymer SPEs is the starting point to discussing conductivity anisotropy. Gomez *et al.* studied the Li^+ distribution in a Polystyrene-*b*-PEO (PS-*b*-PEO) block copolymer SPE with lamellar morphology using energy-filtered transmission electron microscopy.[116] The elemental mapping of the block copolymer SPE cross-section reveals that lithium ions are preferentially located at the center region of the PEO domains. This is because the PEO chains are stretched at the interface and this extended conformation is unfavorable for EO/Li$^+$ coordination, leading to an exclusion of the ions away from the PEO-PS interfacial region.

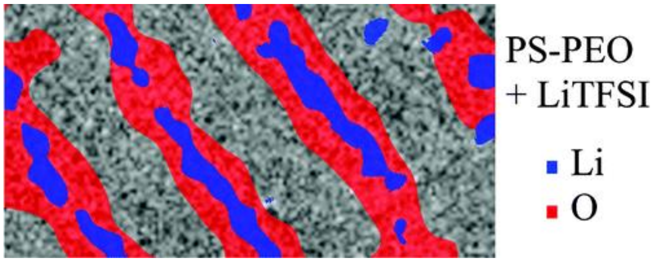

Figure 8. Elemental mapping of a PS-PEO block copolymer SPE doped with LiTFSI. Reprinted with permission from *Nano Letters*, 2009, 9, 1212-1216. Copyright (2009) American Chemical Society.

The chain stretching effect at the interface of the two blocks and uneven ion distribution suggest a fundamental difference in ion conduction mechanism between block copolymer SPE and homopolymer SPE. As discussed earlier, the ion conduction mechanism in homopolymer electrolyte systems is mainly governed by the polymer segmental motion. The cation mobility initially decreases with the increase of M_w and becomes nearly independent of M_w above the M_c (3200 g/mol for PEO), which is consistent with the M_w dependence on T_g. However, the ionic conductivity shows a complex dependence on the molecular weight in the block copolymer SPE case. Balsara and co-workers have systematically studied the M_w effect in a lamella–forming PEO–PS block copolymer electrolyte doped with LiTFSI.[57, 116, 117, 134] In the low M_w region where M_{SEO} is below 10 kg/mol, all the ions are confined in the interfacial zone, and the ion conduction is affected by at least two competing factors: T_g of the PS block and the width of the conducting PEO channel, and the net effect results in a weak linear declining trend of the normalized conductivity as a function of M_{SEO}. When M_{SEO} is above 10 kg/mol, the interfacial effect becomes negligible and the normalized conductivity exhibits a sigmoidal increase with increasing M_w due to the increased fraction of the "free" PEO conducting channel. Ganesan *et al.* employed coarse-grained simulations of the sorption and transport of penetrant cations to study the M_w dependence of conductivity of homopolymer and block copolymer SPE.[135] They showed that in homopolymer SPE, diffusivity effects associated with the free ends of the polymers play an important role. In block copolymer lamellae, the interfacial zone between the blocks presents hindered ion diffusivity and is dependent on molecular weight.

4.2 Alignment and conductivity anisotropy in BCP SPE

In addition to the altered phase behavior and nonuniform distribution of ions in the PEO domain, the nonconductive domain of the block copolymer apparently blocks ion transport, which leads to anisotropic ion transport. Gwee *et al.* reported anisotropic conducting behavior in a PS-*b*-Poly(methyl methacrylate) (PS-*b*-PMMA)/ 1-ethyl-3-methylimidazolium bis (trifluoromethylsulfonyl)imide (EMIm-TFSI) blend system.[136] Young *et al.* investigated the correlation between sample processing conditions and the corresponding ionic conductivity using $LiClO_4$ doped PEO-*b*-PS, where PEO is the majority domain.[137] The SPE samples were hot pressed into disks under vacuum. The authors also cut the disks into ~ 0.5 mm wide strips, which were turned 180° and 90° with respect to the axial direction of each strip, and repacked. They found that for a lamella–forming sample, the moderate shear created during hot-pressing can orient domains perpendicular to the compression force direction and led to as much as 2.5 times decrease in the through-plane conductivity. However, for a hot-pressed cylinder-forming sample, conductivity was not affected by the domain orientations due to the 3-D conducting pathway of the PEO matrix.

Park *et al*. systematically studied the alignment effect on conductivity in proton-conducting domains in hydrated poly(styrenesulfonate-*b*-methylbutylene) copolymer films using several approaches, including solvent casting, hot pressing, and applying external forces such as electric field, or mechanical shearing.[138] The alignment of lamellae was quantified by a combination of 2D SAXS, birefringence, and TEM. Quantitative relationships between domain orientations and transport properties were obtained via in–plane and normal–to–plane proton conductivity measurements of aligned samples. They showed that the pressed sample had highly anisotropic proton conduction with A = 75. Electric field and shear flow alignment lead to an A of ~ 1.3 and 1.4, respectively.

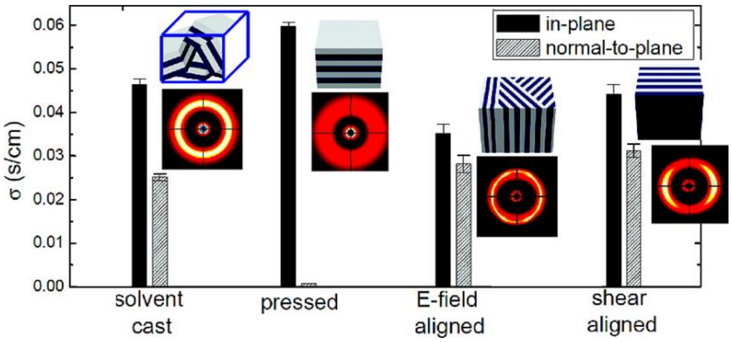

Figure 9. The equilibrium in-plane and normal-to-plane conductivity values of as-cast and aligned samples.[138] Reprinted with permission from *Macromolecules*, 2009, 43, 292-298.Copyright (2009) American Chemical Society.

The conductivities in block copolymer SPEs are often estimated using the effective medium theory (EMT).[139] Based on EMT, if one assumes that the ions are only located in one phase, the effective conductivity σ can be written as:

$$\sigma = f\phi_c\sigma_0 \qquad (3)$$

Where σ_0 and ϕ_c are the intrinsic conductivity and the volume fraction of the conducting phase, and f is the morphological factor. For lamellar block copolymers, $f = 2/3$, and 1/3 for hexagonally packed cylinder structures. Note that this conclusion is based on the following assumptions: i) the length scale of the heterogeneities is much less than the length scale of the medium; ii) the orientations of the small-scale domains are uncorrelated; and iii) the interaction at the domain interfaces can be neglected. Numerous reports have shown that the morphological factor may be much smaller than the values predicted by both theories, ranging from 0.01 – 0.67,[140, 141] and the discrepancies are typically attributed to the poor connectivity between microdomains, which leads to lower measured conductivity for isotropic samples.[140, 142]

Liquid crystal (LC) directed block copolymer alignment appears to be a more efficient approach to enhance conductivity anisotropy.[58, 59, 140, 143-146] Kishimoto reported a macroscopically oriented LC polymeric film with a layered nanostructure prepared by in-situ photopolymerization. The ethylene oxide segment was selectively doped with $LiSO_3CF_3$ for ion conduction and the mesogenic core induced the self-assembly.[59] The electrolyte membrane was spontaneously aligned perpendicular to the glass or ITO substrate when cooled from the isotropic to smectic A phases, and conductivity anisotropies as high as ~ $4.5\text{x}10^3$ were observed at 35 °C, indicating that the ion conduction is efficiently confined within the layer. However, the degree of alignment is limited to the micrometer scale along the thickness direction and none of the studies had compared the in–plane conductivity of the aligned SPE with the isotropic or intrinsic conductivity values.

Alignment of the micro-domains leads to an improvement of the ionic conductivity by creating continuous conducting pathways for directional ion transport. Li *et al.* reported an anisotropy in lithium ion conductivity in phase–segregated LC diblock copolymer PEO-*b*-

PMA(Az) membranes containing mesogene azobenzene units, 11-[4-(4′-butylphenyl-azo)phenoxy]-undecyl methacrylate PMA(Az)[144, 147] with perpendicularly oriented PEO cylindrical domains as ion transport channels (Figure 10a-c). Selective doping of lithium salts into the PEO cylindrical domains was achieved by mixing an appropriate amount of $LiCF_3SO_3$ with 4 wt.% of toluene solution containing the copolymer, then coating onto the desired substrate, and annealing at 140 °C for 24 h. The microphase segregation forces the PEO cylindrical domains containing the lithium salt to be hexagonally arranged and normally oriented in the PMA(Az) domain matrix. Figure 10d,e shows the atomic force microscopy (AFM) top and cross-sectional images of the phase separated SPE. Most of the cylinders with a diameter of around 11 nm can span the entire membrane, *i.e.*, from one interface to the other. Figure 10f shows the temperature dependence of the ionic conductivities perpendicular ($\sigma_{\perp}$) and parallel ($\sigma_{\parallel}$) to the substrate at two salt concentrations. At an O/Li molar ratio of 20:1, the perpendicular conductivity initially increases with the increasing temperature. Above the transition temperature from the smectic A to the isotropic phase, the perpendicular conductivity abruptly drops. The same tendency was observed at the higher salt concentration (O/Li molar ratio = 4:1), although the increase in $\sigma_{\perp}$ conductivity was not as high as expected. On the contrary, the parallel conductivity behaves in a different manner, exhibiting a monotonous increase with increasing temperature for O/Li molar ratios of 20:1 and 4:1. The maximum anisotropy *A* reaches 450 and 40 for O/Li molar of 20:1 and 4:1, respectively.

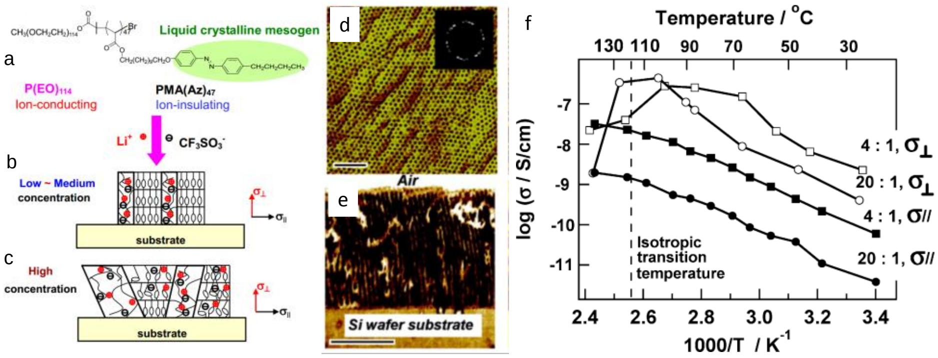

Figure 10. Schematic drawing of structure evolution of diblock copolymer complexes PEO$_{114}$-b-PMA(Az)$_{47}$+LiCF3SO3 at low – medium and high salt concentrations. (a) Chemical structure of the block copolymer, (b) At low and medium salt concentration, selective complexation of Li$^+$ with PEO phase leads to the formation of ordered array of ion-conducting PEO nanocylinders, which are perpendicular to the substrate surface, (c) At high salt concentration, the lithium salt dissolved in both PEO and PMA(Az)$_{47}$ domains, depresses liquid crystalline ordering and disturbs phase segregation of diblock copolymer. (d),(e) Top and cross-sectional AFM phase images of PEO$_{114}$-*b*-PMA(Az)$_{47}$ + LiCF$_3$SO$_3$ membranes (EO : Li$^+$ = 20). (f) Corresponding conductivity. Aadapted with permission from *Macromolecules*, 2007, 40, 8125-8128. Copyright (2007) American Chemical Society.

Osuji and co-workers reported macroscopic alignment of LC-block copolymer SPE using magnetic fields.[58, 140, 145, 146, 148-150] Figure 11 shows an example of the structure of a poly(ethylene oxide-b-6-(4'-cyanobiphenyl-4-yloxy)-hexyl methacrylate) PEO-*b*-PMA/CB block copolymer membrane. LiClO$_4$ was selectively doped into the PEO cylindrical domains for ion conduction and the alignment of PEO cylinders was directed by the smectic poly(MA/CB) block upon magnetic field exposure.

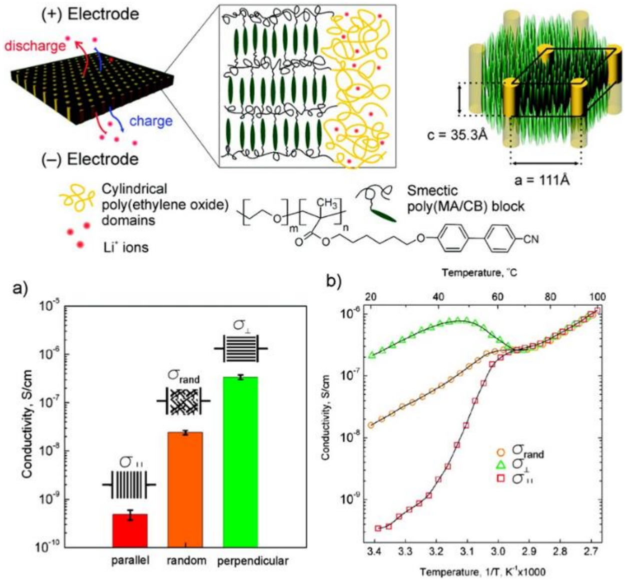

Figure 11. Structure of the poly(ethylene oxide-*b*-6-(4'-cyanobiphenyl-4-yloxy)-hexyl methacrylate) PEO-*b*-PMA/CB block copolymer membrane doped with $LiClO_4$ (top); a) Room temperature ionic conductivities and b) temperature dependent conductivity plots of random and aligned block copolymer SPE along two orthogonal directions.[58] Reprinted with permission from *J. Am. Chem. Soc.*, 2010, 132, 17516-17522. Copyright (2010) American Chemical Society.

In this work, the parallel (//) and perpendicular (⊥) directions were defined as the PEO cylinders parallel and orthogonal to the electrode surface, respectively. The conductivity anisotropy *A* reached ~ 10^3 under 5T magnetic field, suggesting the effective blocking of ion migration transverse to the PEO cylinder long axis direction. Interestingly, a nearly 10-fold increase of the $\sigma_\perp$ compared with that of isotropic SPE was observed, which deviated from the expected 2-fold increase based on the morphological argument predicted by EMT. This discrepancy suggests that the less ideal connectivity at the grain boundaries may have caused the conductivity decrease in the isotropic LC block copolymer SPE.

5. Mechanical field induced anisotropic ion transport

Conductivity anisotropy has also been found in stretched semi-crystalline PEO SPEs.[61, 151-158] Golodnitsky and co-workers reported stretching induced conductivity enhancement by a factor of 5 to 40 in several $P(EO)_nLiX$ (X= I, CF_3SO_3, TFSI, BOB) electrolytes.[61, 151-153, 158] In these studies, the hot pressed electrolyte membranes were uniaxially stretched under 450-500 N/cm^2 load at elevated temperatures and the *in-situ* longitudinal conductivity was monitored. Stretching induces the unraveling of loops in the polymer molecules and enhances the chain alignment along the direction of applied force. Despite a decrease of polymer segmental motion, it was suggested that Li^+ hopping along the helix is facilitated by the long range order, as supported by the enhanced Li^+ diffusivity measured by Li NMR and the decreased activation energy obtained from Arrhenius plot. A maximum conductivity anisotropy of 40 was observed in a concentrated semi-crystalline electrolyte $P(EO)_7LiI$, in which the partial alignment of the PEO helices in the crystalline phase was believed to be responsible for the conductivity enhancement.

Li *et al.* used multi-axis pulsed-field-gradient NMR to measure diffusion anisotropy to probe the orientational order as a function of water content and membrane stretching in a uniaxially stretched Nafion film.[159] They showed that transport anisotropy depends linearly on the degree of alignment: with increased alignment, substantial enhancement in water transport along the draw direction and suppression in the transverse direction was achieved. Dong *et al.* fabricated Nafion nanofibers using electrospinning and showed that a high proton conductivity value of 1.5 S/cm was achieved. X-ray scattering showed oriented ionic domains in the nanofiber, which account for the enhanced ion conductivity.[160]

6. Anisotropic ion transport in hybrids/nanocomposite SPE

6.1. SPE containing low dimensional particles

Another widely studied approach to address both conductivity and mechanical properties is based on PEO–ceramic nanocomposite SPEs. The incorporation of certain ceramic fillers with Lewis acid characteristic such as TiO_2, SiO_2, or Al_2O_3 has been shown to enhance both ionic conductivity and mechanical properties of the SPE.[26, 29-31, 60, 161-176] During the early investigations, Scrosati and co-workers showed that the addition of micro-sized ceramic particles γ-$LiAlO_2$ into a $P(EO)_8LiClO_4$ SPE improved the mechanical properties, interfacial stability and ionic conductivity;[161] however, the mechanism of this enhancement was not well understood. Follow-up studies suggest that ceramic particles with nanoscale particle sizes can result in even better performance, and the ion conduction mechanism in these nanocomposite SPE was systematically studied. [29-31, 165, 167, 170] It was suggested that the ceramic nanoparticles with Lewis acid characteristics are competing with lithium cations to form complexes with PEO. Hanson *et al.* suggested that the ion mobilities are correlated to the nanoparticle–induced changes in the polymer segmental dynamics.[177] On the other hand, Chung *et al.* reported that the cation transference number t^+ for their nanocomposite SPE (0.5-0.6 for SPE containing TiO_2) was considerably higher than their ceramic-free SPE (usually 0.2-0.3), and the cation diffusivity measured by NMR methods was nearly one order of magnitude higher in the nanocomposite SPE.[31] These evidences likely suggest that the specific Lewis acid–base interactions among the ceramic surface groups, lithium salt, and the polymer segments facilitate the ion dissociation and possibly create preferential conducting pathways at the boundaries of the ceramic particles, promoting Li^+ transport.

The types of functional groups on the surface of the ceramic particles play a critical role to the ion conduction in nanocomposite SPEs. In a study conducted by Croce *et al*., three types of Al_2O_3 nanoparticles with acidic, neutral and basic surface characteristics were incorporated into a $P(EO)_{20}LiSO_3CF_3$ SPE.[170] The acidic and neutral Al_2O_3 based SPEs showed higher degrees of conductivity enhancement over the basic Al_2O_3 SPE, leading the author to propose the mechanism to be the specific Lewis-acid interactions. Acidic/neutral Al_2O_3 forms hydrogen bonding with the anions as well as the ether oxygens on PEO chains, promoting the salt dissociation and weakening the cation-polymer coordination, while the basic Al_2O_3 can only interact with Li^+; however, the study conducted by Jayathilaka *et al.* on a $P(EO)_9LiTFSI$ SPE system suggests that there is no direct interaction between the filler particles and the polymer chain. The Al_2O_3 particles interact with both cations and anions, providing additional sites for ion hopping. In this case, the degree of conductivity improvement provided by the nanoparticles followed the order: acidic > basic > neutral > weakly acidic > filler free.[171] Another study on a low M_w PEG–$LiClO_4$–Al_2O_3 system showed that the neutral fillers gave higher conductivity compared with acidic and basic fillers.[168] There is no clear trend of surface group type versus conductivity enhancement, and it seems the specific interactions also depend on the type of anions and the polymer matrix being used.

Although the nanocomposite approach for novel SPE development appears to be promising, the conductivity enhancement due to the nanoparticles is not universal and contradictory results have been found in other SPEs. Best *et al.* found no improvement, and even a decrease of conductivity in some fully amorphous polyether based SPEs with the addition of TiO_2 or Al_2O_3 nanoparticles.[178] Johansson *et al.* reported no significant influence of the SiO_2 fillers on amorphous PEO-LiTFSI SPEs.[179] Xie *et al.* studied a PEO–LiTFSI SPE containing fumed silica nanoparticles, and conductivity of the composite SPE was found to be decreased above T_m when compared with an ultrapure PEO SPE.[180] Depending on the type of anions, the nature of the nanoparticles and the structure and molecular weight of the polymer, different ion conduction mechanisms may be proposed.

Besides the multi-phase nanocomposite SPE, a few mono-phase hybrid SPEs have also been studied, including 3D hybrid inorganic organic network SPE and Zeolitic inorganic-organic SPE.[181-186] In these systems either metal, non-metal atoms or inorganic clusters are bridged by organic molecules to form ion-conducting materials. Detailed reviews on those systems can be found elsewhere.[187, 188]

6.2. Two-dimensional nanoplatelets induced conductivity anisotropy

While the effect of 0-dimensional (0D) nanoparticles on the ionic conductivity of the SPE is still under debate, it is evident that introducing 2-dimensional (2D) nanoplates can induce conductivity anisotropy in the resultant SPE systems. Montmorillonite and hectorite, as charged layer (2D) silicates, have been compounded with polymer ion hosts using solution infiltration, melt blending and layer–by–layer (LbL) assembly methods to fabricated hybrid SPE. For PEO / montmorillonite composites, Ruiz- Hitzky *et al.* demonstrated conductivity enhancement in the hybrid SPE, and attributed this enhancement to increased layer separation, a factor associated with relaxations of the polymer chain.[189, 190] It was suggested that the polymer weakens the interactions between the cation and the negatively charged clay surface, thereby increasing conductivity. A conductivity anisotropy of approximately 100 for polyphosphazene-montmorillonite SPE was reported by Hutchison *et al.*[191] Lutkehaus *et al.* using an LbL method to fabricate hybrid SPE comprised of poly(ethylene imine) (PEI), laponite clay, and PEO (Figure

12).[192] What was unique in their system is that PEI/Li-clay/PEO forms trilayers; each trilayer was approximately 5 nm thick, and clay platelets were controlled to be parallel with the substrate. Anisotropic ion transport, resulting from the anisotropic structure, was demonstrated with a conductivity anisotropic factor of ~ 100. They also showed that the activation energy associated with ion transport in (PEI/Li-clay/PEO) (0.35-0.37 eV) was similar to that of lithium cations in PEO.

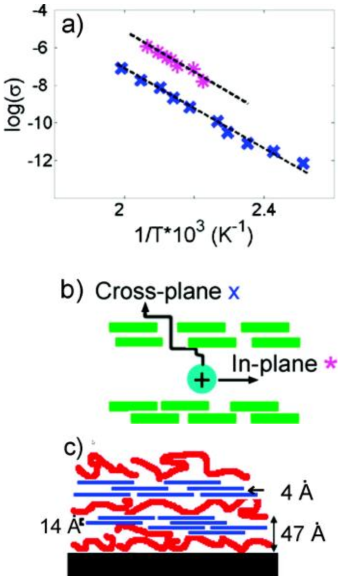

Figure 12. (a) Arrhenius plot of the variation of conductivity with temperature. In-plane conductivity (pink *) is ~ 100 times higher than cross-plane conductivity (blue x). (b) Schematics showing that cross-plane ion conduction is hindered by the presence of ordered clay nanoplatelets. (c) Proposed structure of PEI/Li-clay/PEO LbL assembly. The trilayer thickness is 4.7 nm, basal spacing 1.4 nm, and gallery spacing 0.4 nm.[192] Reprinted with permission from *Langmuir*, 2007, 23, 8515-8521. Copyright (2007) American Chemical Society.

7. Holographic polymerization

Holographic polymerization (HP) has been used to fabricate tunable periodic nanostructured membranes with long-range order and low defect content.[193] Recently it has been demonstrated that this versatile technique can be used to fabricate novel electrolyte membranes with both robust mechanical properties and highly ordered conducting channels. During the photopolymerization process, a mixture of photopolymerizable monomers, initiator, and inert components are exposed to an interference pattern generated by two or more coherent beams. The monomers diffuse into the light, or constructive region, and start to cross-link, while all the inert components are partitioned into the dark, destructive interference volumes. Depending on the geometry of the optical setups, 1D, 2D or 3D nanostructure with tunable spacing can be readily patterned. HP structures can be used in various exciting applications.[194, 195] Due to incorporation of inert materials, a diversity of polymer composite systems can be fabricated in a top-down manner with unprecedented structural control. Using soft matter, such as LCs as the inert material, leads to the formation of holographic polymer dispersed liquid crystals whose band gap can be tuned by electric fields and mechanical strain.[195] Hierarchically ordered gratings have also been achieved by using block copolymers as the inert materials.[144, 196-198] Using HP, we recently demonstrated creating long range ordered ~100 nm nano-channels of electrolyte comprised of Norland 65, PEO and bis trifluoromethanesulfonimide lithium salt (LiTFSI) at a Li:EO ratio of 1:19, and termed the membranes holographic polymer electrolyte membranes (hPEMs).[62] The volume fraction of electrolyte was varied from 29 to 55 v/v %, and a variety of morphologies were observed. At lower electrolyte loadings, ~50-200 nm droplets were formed in well-confined 1D layers. Droplet growth, coalescence and deformation from photopolymer impingement within these layers as the electrolyte loading was increased up to 45-50 v/v % was observed in TEM, shown in Figure 13. Upon further loading of the electrolyte, the thermodynamics of the system limited the formation ability of the grating, and an ordered assembly of electrolyte droplets is barely evident in the TEM images.

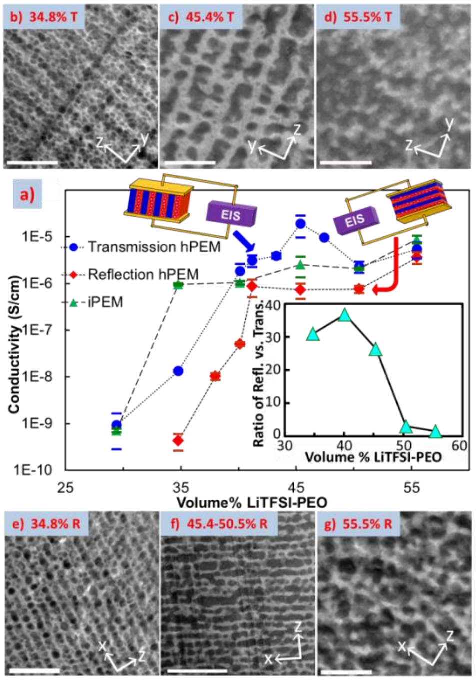

Figure 13. EIS conductivity with respect to electrolyte v/v % loading measured in the films' z direction (a) and TEM images of corresponding transmission gratings (b-d) and reflection gratings (e-g) with corresponding electrolyte v/v % with scale bars of 1 µm.[62] Reprinted with permission from *Nano letters*, 2011, 12, 310-314. Copyright (2011) American Chemical Society.

Electrochemical impedance spectroscopy (EIS) was used to determine the ionic conductivity of the films at room temperature, shown in Figure 13. Both through- and in-plane measurements displayed a percolation-like behavior that increased the conductivity by ~3 orders of magnitude. The in-plane conductivities were consistently higher than the reflection gratings', and achieved a maximum anisotropy of 38, which was a 3-fold improvement over one-step thin film synthesis techniques at time of publication. This consistent anisotropic behavior is clear evidence for effective ion-confinement and channel formation.

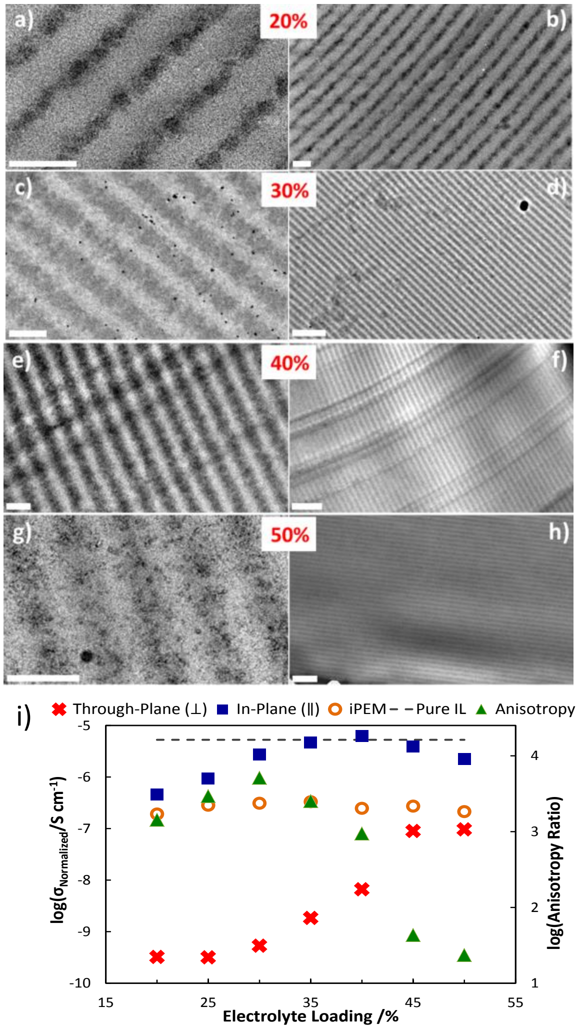

Figure 14. TEM images of hPEMs. (a), (c), (e), and (g) Micrographs of 20-50 w/w% electrolyte with a scale bar of 200 nm. (b), (d), (f), and (h) Micrographs with a scale bar of 1 µm. All samples were ultra-microtomed stained with RuO_4. (i) Ionic conductivity measured via EIS normalized by IL volume fraction versus electrolyte content of hPEMs for parallel (blue squares), perpendicular (red crosses) and isotropically polymerized membranes (orange circles) at room temperature. Anisotropic ratio of in-plane versus through-plane is shown in green triangles. Error bars are on the same scale as the symbols. Reprinted from *J. Pow. Sour.*, 2014, 271, 597-603. Copyright (2014), with permission from Elsevier.

However, while already a 3-fold improvement over one-step thin film synthesis techniques, much available improvement exists by optimizing the morphology beyond a semi-continuous brick-and-mortar structure. In HP, the final morphology can be controlled by tuning the phase separation and photopolymerization kinetics. To this end, we used trihexyltetradecylphosphonium bromide (BrTHTDP) ionic liquid (IL) to replace the PEO/LiTFSI system.[199] Figure 14 shows TEM images of various electrolyte loadings, where the dark domains are IL-rich regions and the lighter domains are cross-linked NOA65. Phase separated, defect free, and long-range continuous layers for both the IL and NOA65 can be seen clearly in all the samples. “Cross talk” of adjacent layers was not observed for either domain in any film characterized. Normalized conductivities for in plane and through plane directions, and the resulting ionic conductivity anisotropy versus electrolyte loading, are also shown in Figure 14. $\sigma_{\parallel}$ varies moderately with increasing IL concentration and a maximum normalized conductivity is seen at 40 w/w% with $6.24\cdot10^{-6}$ S/cm, which is comparable to the pure IL conductivity of $5.28\cdot10^{-6}$ S/cm. Increasing or decreasing the IL loading from this ratio decreases the normalized conductivity, suggesting optimal partitioning at this loading. $\sigma_{\perp}$ is lower than $\sigma_{\parallel}$ for all the hPEMs; it significantly rises with electrolyte loading, and experiences a weak percolation-like behavior at 45 w/w% loading. As a result, from 20 w/w%, the anisotropy increases to 5120 at 30 w/w% and then decreases to ~ 20 for 45 w/w % hPEM. Clearly, the relatively clean phase separation also results in the extremely high conductivity anisotropy between the in-plane and through-plane directions; the homogeneous NOA65-rich layer “blocks” the through-plane ion transport. This control is governed by two factors: the concentration of ions in the NOA-rich layer, and the decrease of ion mobility caused by an increase in viscosity, which hinders ion flux. As the NOA65 monomer loading is decreased, the thickness of the NOA-rich layer decreases and the volume fraction of trapped ions increases. At a certain NOA-layer thickness and ion volume fraction, the ions are able to percolate through the depth of the NOA65 blockade.

8. Summary and outlook

In this article, we briefly summarized the anisotropic ion transport in five types of SPE, namely semicrystalline, block copolymer, mechanically stretched, hybrids/nanocomposites, and holographic polymerized SPEs. Such anisotropy typically arises from nanoscale morphology and plays a significant role in SPE performance. Despite four decades of extensive work in SPEs, the detailed structures and dynamic nature of ion containing SPEs are still not clear; the intertwined structural and dynamic effects of polymer chains on ion transport and the altered phase behaviors of polymers upon ion doping all factor into the complex behavior of SPEs. From a scientific point of view, it is intriguing to investigate the phase structures and dynamics of these complex SPEs. From a technological standpoint, one has to be mindful of both the potential and limitations in the reported systems. For each system, there are challenges and opportunities:

Semicrystalline SPE: Our discussion showed that crystalline lamellae in semicrystalline SPE confine and direct ion transports. Therefore, anisotropic crystalline morphology can be correlated directly with anisotropic ion transport. In order to design SPEs for practical applications, high through plane ion conduction is needed, which dictates the lamellae must be perpendicular to the polymer electrolyte membrane. External fields or epitaxy growth may be employed for this particular purpose.

Block copolymer SPE: Block copolymer SPEs have been widely studied. The nonconducting domain of the block copolymer can be used to direct ion transport. Well aligned block copolymer nanomorphology leads to highly anisotropic ion conduction, and mitigate the domain contact effect that could reduce ion conductivity. The next challenge is achieving large scale aligned block copolymers in an energetically economical manner.

Mechanically field: Mechanical fields can induce conductivity anisotropy and can be implemented easily based on today's industry setting, though the conductivity anisotropy is relatively small compared with other methods. More importantly, however, using this method leads to the faster ion transport direction being perpendicular to the film, which is orthogonal to the preferred transport direction for most applications.

Hybrids/nanocomposites: Incorporating inorganic fillers to fabricate hybrd/nanocomposite SPE has shown promise in both mechanical property and ion conductivity enhancement. Although there are debates on detailed mechanisms, using 2D or 1D nanofillers to guide ion transport in SPEs is an interesting direction to pursue. Given the variety of nanofillers available, it is anticipated that research activities in the direction will grow further.

Holographic polymerized SPE: Holographic polymerized SPEs are a relatively new approach; nevertheless, unprecedented ion transport anisotropy has been demonstrated. Considering defect-free nanostructure can be fabricated within a fraction of minutes, this novel system might lead to a library of interesting SPEs. The clearest challenge in this direction is how to scale up the nanomanufacturing process to generate large scale membranes.

It is promising for achieving high through plane room temperature conductivity while maintaining good mechanical properties by tuning SPE nanomorphologies in systems such as block copolymer, nanoparticle containing, and holographic polymerized SPE. While ion conductivity, phase structure, and mechanical properties of SPEs have been extensively studied, more battery testing experiments need to be conducted to validate the end device performance.

Acknowledgements

CYL is grateful for the support from the National Science Foundation over the years through grants CMMI-1100166, EEC 1138240, CMMI-1200385, CMMI-1334067, DMR-1308958, and CBET 1438240. DMS would like to acknowledge the NSF IGERT and GRFP fellowship support.

References

1. J. M. Tarascon and M. Armand, *Nature*, 2001, **414**, 359-367.
2. M. Armand and J. M. Tarascon, *Nature*, 2008, **451**, 652-657.
3. I. Stepniak and E. Andrzejewska, *Electrochimica Acta*, 2009, **54**, 5660-5665.
4. A. M. Stephan, *European Polymer Journal*, 2006, **42**, 21-42.
5. J. Y. Song, Y. Y. Wang and C. C. Wan, *Journal of Power Sources*, 1999, **77**, 183-197.
6. E. Quartarone and P. Mustarelli, *Chem. Soc. Rev.*, 2011, **40**, 2525-2540.
7. A. Lewandowski and A. Swiderska-Mocek, *Journal of Power Sources*, 2009, **194**, 601-609.
8. J. Le Bideau, L. Viau and A. Vioux, *Chemical Society Reviews*, 2011, **40**, 907-925.
9. M. A. Hickner, *Mater. Today*, 2010, **13**, 34-41.
10. M. B. Herath, S. E. Creager, R. V. Rajagopal, O. E. Geiculescu and D. D. DesMarteau, *Electrochimica Acta*, 2009, **54**, 5877-5883.
11. J. B. Goodenough and Y. Kim, *Chem. Mater.*, 2010, **22**, 587-603.
12. P. G. Bruce, B. Scrosati and J. M. Tarascon, *Angew. Chem.-Intern. Ed.*, 2008, **47**, 2930-2946.
13. D. T. Hallinan, Jr. and N. P. Balsara, *Annual Review of Materials Research, Vol 43*, 2013, **43**, 503-+.
14. D. E. Fenton, J. M. Parker and P. V. Wright, *Polymer*, 1973, **14**, 589-589.
15. P. V. Wright, *British Poly. J.*, 1975, **7**, 319-327.
16. P. V. Wright, *J. P. Sci.: Polymer Phys. Ed.*, 1976, **14**, 955-957.
17. A. Killis, J.-F. Le Nest and H. Cheradame, *Die Makromolekulare Chemie, Rapid Communications*, 1980, **1**, 595-598.
18. C. C. Lee and P. V. Wright, *Polymer*, 1982, **23**, 681-689.
19. D. R. Payne and P. V. Wright, *Polymer*, 1982, **23**, 690-693.
20. C. Berthier, W. Gorecki, M. Minier, M. B. Armand, J. M. Chabagno and P. Rigaud, *Solid State Ionics*, 1983, **11**, 91-95.

21. K. Murata, S. Izuchi and Y. Yoshihisa, *Electrochimica Acta*, 2000, **45**, 1501-1508.
22. W. H. Meyer, *Adv. Mater.*, 1998, **10**, 439-448.
23. S. Takeoka, H. Ohno and E. Tsuchida, *Polymers for Advanced Technologies*, 1993, **4**, 53-73.
24. M. A. Ratner and D. F. Shriver, *Chem. Rev.*, 1988, **88**, 109-124.
25. E. Quartarone and P. Mustarelli, *Chem. Soc. Rev.*, 2011, **40**, 2525-2540.
26. E. Quartarone, P. Mustarelli and A. Magistris, *Solid State Ionics*, 1998, **110**, 1-14.
27. W. S. Young, W. F. Kuan and T. H. Epps, *J. P. Sci. Part B: Poly. Phys.*, 2014, **52**, 1-16.
28. Y. A. Elabd and M. A. Hickner, *Macromolecules*, 2011, **44**, 1-11.
29. F. Croce, G. B. Appetecchi, L. Persi and B. Scrosati, *Nature*, 1998, **394**, 456-458.
30. F. Croce, L. Persi, F. Ronci and B. Scrosati, *Solid State Ionics*, 2000, **135**, 47-52.
31. S. Chung, Y. Wang, L. Persi, F. Croce, S. Greenbaum, B. Scrosati and E. Plichta, *J. Power Sources*, 2001, **97**, 644-648.
32. Z. Gadjourova, Y. G. Andreev, D. P. Tunstall and P. G. Bruce, *Nature*, 2001, **412**, 520-523.
33. Z. Stoeva, I. Martin-Litas, E. Staunton, Y. G. Andreev and P. G. Bruce, *J. Am. Chem. Soc.*, 2003, **125**, 4619-4626.
34. A. M. Christie, S. J. Lilley, E. Staunton, Y. G. Andreev and P. G. Bruce, *Nature*, 2005, **433**, 50-53.
35. A. L. Agapov and A. P. Sokolov, *Macromolecules*, 2011, **44**, 4410-4414.
36. Y. Wang, A. L. Agapov, F. Fan, K. Hong, X. Yu, J. Mays and A. P. Sokolov, *Phys. Rev. Lett.*, 2012, **108**, 088303.
37. K. Sinha and J. K. Maranas, *Macromolecules*, 2011, **44**, 5381-5391.
38. K. Sinha, W. Wang, K. I. Winey and J. K. Maranas, *Macromolecules*, 2012, **45**, 4354-4362.
39. G. J. Tudryn, W. Liu, S.-W. Wang and R. H. Colby, *Macromolecules*, 2011, **44**, 3572-3582.
40. K.-J. Lin, K. Li and J. K. Maranas, *RSC Advances*, 2013, **3**, 1564-1571.
41. S. Dou, S. Zhang, R. J. Klein, J. Runt and R. H. Colby, *Chem. of Mater.*, 2006, **18**, 4288-4295.
42. W. Wang, G. J. Tudryn, R. H. Colby and K. I. Winey, *J. Am. Chem. Soc.*, 2011, **133**, 10826-10831.
43. D. Fragiadakis, S. Dou, R. H. Colby and J. Runt, *J. Chem. Phys.*, 2009, **130**, -.
44. K.-J. Lin and J. K. Maranas, *Macromolecules*, 2012, **45**, 6230-6240.
45. M. B. Armand, *Annual Review of Materials Science*, 1986, **16**, 245-261.
46. F. Vögtle and E. Weber, eds. S. Patai and Z. Rappoport, Wiley, New York, 1989, ch. 4.
47. C. J. Pedersen, *Ange. Chem. Int. Ed. in Eng.*, 1988, **27**, 1021-1027.
48. M. Armand, *Solid State Ionics*, 1983, **9–10, Part 2**, 745-754.
49. D. Baril, C. Michot and M. Armand, *Solid State Ionics*, 1997, **94**, 35-47.
50. M. Armand, *Adv. Mater.*, 1990, **2**, 278-286.

51. K. Xu, *Chem. Rev.*, 2004, **104**, 4303-4418.
52. M. Ue, *J. Electrochem. Soc.*, 1994, **141**, 3336-3342.
53. M. Park, X. Zhang, M. Chung, G. B. Less and A. M. Sastry, *J. Power Sources*, 2010, **195**, 7904-7929.
54. C. Monroe and J. Newman, *J. Electrochem. Soc.*, 2005, **152**, A396-A404.
55. C. Wang, T. Sakai, O. Watanabe, K. Hirahara and T. Nakanishi, *J. Electrochem. Soc.*, 2003, **150**, A1166-A1170.
56. T. Niitani, M. Shimada, K. Kawamura and K. Kanamura, *J. Power Sources*, 2005, **146**, 386-390.
57. M. Singh, O. Odusanya, G. M. Wilmes, H. B. Eitouni, E. D. Gomez, A. J. Patel, V. L. Chen, M. J. Park, P. Fragouli, H. Iatrou, N. Hadjichristidis, D. Cookson and N. P. Balsara, *Macromolecules*, 2007, **40**, 4578-4585.
58. P. W. Majewski, M. Gopinadhan, W.-S. Jang, J. L. Lutkenhaus and C. O. Osuji, *J. Am. Chem. Soc.*, 2010, **132**, 17516-17522.
59. K. Kishimoto, M. Yoshio, T. Mukai, M. Yoshizawa, H. Ohno and T. Kato, *J. Am. Chem. Soc.*, 2003, **125**, 3196-3197.
60. H. J. Walls, J. Zhou, J. A. Yerian, P. S. Fedkiw, S. A. Khan, M. K. Stowe and G. L. Baker, *J. Power Sources*, 2000, **89**, 156-162.
61. D. Golodnitsky, E. Livshits, A. Ulus, Z. Barkay, I. Lapides, E. Peled, S. H. Chung and S. Greenbaum, *J. Phys. Chem. A*, 2001, **105**, 10098-10106.
62. D. M. Smith, B. Dong, R. W. Marron, M. J. Birnkrant, Y. A. Elabd, L. V. Natarajan, V. P. Tondiglia, T. J. Bunning and C. Y. Li, *Nano letters*, 2011, **12**, 310-314.
63. D. J. Bannister, G. R. Davies, I. M. Ward and J. E. McIntyre, *Polymer*, 1984, **25**, 1291-1296.
64. N. Kobayashi, M. Uchiyama and E. Tsuchida, *Solid State Ionics*, 1985, **17**, 307-311.
65. R. Bouchet, S. Maria, R. Meziane, A. Aboulaich, L. Lienafa, J.-P. Bonnet, T. N. T. Phan, D. Bertin, D. Gigmes, D. Devaux, R. Denoyel and M. Armand, *Nat Mater*, 2013, **12**, 452-457.
66. C. D. Robitaille and D. Fauteux, *J. Electrochem. Soc.*, 1986, **133**, 315-325.
67. R. Neat, M. Glasse, R. Linford and A. Hooper, *Solid State Ionics*, 1986, **18–19, Part 2**, 1088-1092.
68. M. Marzantowicz, J. R. Dygas, F. Krok, A. Łasińska, Z. Florjańczyk, E. Zygadło-Monikowska and A. Affek, *Electrochimica Acta*, 2005, **50**, 3969-3977.
69. M. Marzantowicz, J. R. Dygas, F. Krok, J. L. Nowiński, A. Tomaszewska, Z. Florjańczyk and E. Zygadło-Monikowska, *J. Power Sources*, 2006, **159**, 420-430.
70. M. Marzantowicz, J. R. Dygas, F. Krok, Z. Florjańczyk and E. Zygadło-Monikowska, *Electrochimica Acta*, 2007, **53**, 1518-1526.
71. M. Marzantowicz, F. Krok, J. R. Dygas, Z. Florjańczyk and E. Zygadło-Monikowska, *Solid State Ionics*, 2008, **179**, 1670-1678.

72. G. Zardalidis, E. Ioannou, S. Pispas and G. Floudas, *Macromolecules*, 2013, **46**, 2705-2714.
73. S. Lascaud, M. Perrier, A. Vallee, S. Besner, J. Prud'homme and M. Armand, *Macromolecules*, 1994, **27**, 7469-7477.
74. G. S. MacGlashan, Y. G. Andreev and P. G. Bruce, *Nature*, 1999, **398**, 792-794.
75. Z. Stoeva, I. Martin-Litas, E. Staunton, Y. G. Andreev and P. G. Bruce, *J. Am. Chem. Soc.*, 2003, **125**, 4619-4626.
76. Z. Gadjourova, D. Martín y Marero, K. H. Andersen, Y. G. Andreev and P. G. Bruce, *Chem. of Mater.*, 2001, **13**, 1282-1285.
77. G. S. MacGlashan, Y. G. Andreev and P. G. Bruce, *Nature*, 1999, **398**, 792-794.
78. E. Staunton, Y. G. Andreev and P. G. Bruce, *Faraday Discussions*, 2007, **134**, 143-156.
79. B.-K. Choi and Y.-W. Kim, *Electrochimica Acta*, 2004, **49**, 2307-2313.
80. M. Marzantowicz, J. R. Dygas, F. Krok, A. Łasińska, Z. Florjańczyk and E. Zygadło-Monikowska, *Electrochimica Acta*, 2006, **51**, 1713-1727.
81. Y. Zhang, J. Li, H. Huo and S. Jiang, *Journal of Applied Polymer Science*, 2012, **123**, 1935-1943.
82. J. R. Dygas, B. Misztal-Faraj, Z. Florjańczyk, F. Krok, M. Marzantowicz and E. Zygadło-Monikowska, *Solid State Ionics*, 2003, **157**, 249-256.
83. M. Minier, C. Berthier and W. Gorecki, *Journal De Physique*, 1984, **45**, 739-744.
84. S. K. Fullerton-Shirey and J. K. Maranas, *Macromolecules*, 2009, **42**, 2142-2156.
85. S. Cheng, D. M. Smith and C. Y. Li, *Macromolecules*, 2014, **47**, 3978-3986.
86. D. Blundell, A. Keller and A. Kovacs, *J. Polym. Sci. B: Polym. Lett.*, 1966, **4**, 481-486.
87. B. Li and C. Y. Li, *J. Am. Chem. Soc.*, 2007, **129**, 12-13.
88. B. B. Wang, B. Li, B. Zhao and C. Y. Li, *J. Am. Chem. Soc.*, 2008, **130**, 11594-11595.
89. C. Y. Li, *J. Poly. Sci. Poly. Phys.*, 2009, **47**, 2436-2440.
90. P. Geil, *Polymer single crystal*, Interscience New York, 1963.
91. B. B. Wang, B. Li, R. C. M. Ferrier and C. Y. Li, *Macromol. Rapid Commun.*, 2010, **31**, 169-175.
92. B. B. Wang, B. Li, B. Dong, B. Zhao and C. Y. Li, *Macromolecules*, 2010, **43**, 9234-9238.
93. B. Li, B. B. Wang, R. C. M. Ferrier and C. Y. Li, *Macromolecules*, 2009, **42**, 9394-9399.
94. L. Li, C. Y. Li and C. Y. Ni, *J. Am. Chem. Soc.*, 2006, **128**, 1692-1699.
95. C. Y. Li, L. Li, W. Cai, S. L. Kodjie and K. K. Tenneti, *Adv. Mater.*, 2005, **17**, 1198-1202.
96. T. Zhou, B. Dong, H. Qi, S. Mei and C. Y. Li, *J. Polym. Sci. Poly. Phys.*, 2014, **52**, 1620-1640.
97. W. Wang and C. Y. Li, *ACS Macro Letters*, 2014, **3**, 175-179.
98. H. Qi, W. Wang and C. Y. Li, *ACS Macro. Lett.*, 2014, **3**, 675-678.
99. E. D. Laird and C. Y. Li, *Macromolecules* 2013, **46**, 2877-2891.
100. B. Dong, T. Zhou, H. Zhang and C. Y. Li, *ACS Nano*, 2013, **7**, 5192-5198.

101. B. Dong, W. Wang, D. L. Miller and C. Y. Li, *J. Mater. Chem.*, 2012, **22**, 15526-15529.
102. B. Dong, D. L. Miller and C. Y. Li, *Journal of Physical Chemistry Letters*, 2012, **3**, 1346-1350.
103. B. Dong, B. Li and C. Y. Li, *J. Mater. Chem.*, 2011, **21**, 13155-13158.
104. L. E. Nielsen, *J. Macromolecular Sci. Part A: Chem.*, 1967, **1**, 929-942.
105. R. K. Bharadwaj, *Macromolecules*, 2001, **34**, 9189-9192.
106. B. Xu, Q. Zheng, Y. Song and Y. Shangguan, *Polymer*, 2006, **47**, 2904-2910.
107. M. Watanabe, S. Nagano, K. Sanui and N. Ogata, *Polym J*, 1986, **18**, 809-817.
108. H. Vogel, *Physikalische Zeitschrift*, 1921, **22**, 645.
109. G. Tammann and W. Hesse, *Zeitschrift für anorganische und allgemeine Chemie*, 1926, **156**, 245-257.
110. G. S. Fulcher, *Journal of the American Ceramic Society*, 1925, **8**, 339-355.
111. A.-V. G. Ruzette, P. P. Soo, D. R. Sadoway and A. M. Mayes, *J. Electrochem. Soc.*, 2001, **148**, A537-A543.
112. F. M. Gray, J. R. MacCallum, C. A. Vincent and J. R. M. Giles, *Macromolecules*, 1988, **21**, 392-397.
113. P. P. Soo, B. Huang, Y.-I. Jang, Y.-M. Chiang, D. R. Sadoway and A. M. Mayes, *J. Electrochem. Soc.*, 1999, **146**, 32-37.
114. A. A. Teran and N. P. Balsara, *Macromolecules*, 2011, **44**, 9267-9275.
115. E. D. Gomez, M. L. Ruegg, A. M. Minor, C. Kisielowski, K. H. Downing, R. M. Glaeser and N. P. Balsara, *Macromolecules*, 2008, **41**, 156-162.
116. E. D. Gomez, A. Panday, E. H. Feng, V. Chen, G. M. Stone, A. M. Minor, C. Kisielowski, K. H. Downing, O. Borodin, G. D. Smith and N. P. Balsara, *Nano Letters*, 2009, **9**, 1212-1216.
117. A. Panday, S. Mullin, E. D. Gomez, N. Wanakule, V. L. Chen, A. Hexemer, J. Pople and N. P. Balsara, *Macromolecules*, 2009, **42**, 4632-4637.
118. N. S. Wanakule, A. Panday, S. A. Mullin, E. Gann, A. Hexemer and N. P. Balsara, *Macromolecules*, 2009, **42**, 5642-5651.
119. N. S. Wanakule, J. M. Virgili, A. A. Teran, Z.-G. Wang and N. P. Balsara, *Macromolecules*, 2010, **43**, 8282-8289.
120. F. S. Bates and G. H. Fredrickson, *Print edition*, 1999, **52**, 32-38.
121. A. J. Meuler, M. A. Hillmyer and F. S. Bates, *Macromolecules*, 2009, **42**, 7221-7250.
122. T. H. Epps, T. S. Bailey, H. D. Pham and F. S. Bates, *Chem. of Mater.*, 2002, **14**, 1706-1714.
123. B.-K. Cho, A. Jain, S. M. Gruner and U. Wiesner, *Science*, 2004, **305**, 1598-1601.
124. W.-S. Young, P. J. Brigandi and T. H. Epps, *Macromolecules*, 2008, **41**, 6276-6279.
125. T. H. Epps, T. S. Bailey, R. Waletzko and F. S. Bates, *Macromolecules*, 2003, **36**, 2873-2881.
126. T. Niitani, M. Shimada, K. Kawamura, K. Dokko, Y.-H. Rho and K. Kanamura, *Electrochem. and Solid-State Lett.*, 2005, **8**, A385-A388.

127. S. H. Kim, M. J. Misner, L. Yang, O. Gang, B. M. Ocko and T. P. Russell, *Macromolecules*, 2006, **39**, 8473-8479.
128. W.-S. Young and T. H. Epps, *Macromolecules*, 2009, **42**, 2672-2678.
129. S. N. Patel, A. E. Javier, K. M. Beers, J. A. Pople, V. Ho, R. A. Segalman and N. P. Balsara, *Nano Letters*, 2012, **12**, 4901-4906.
130. I. Nakamura, N. P. Balsara and Z.-G. Wang, *Phys. Rev. Lett.*, 2011, **107**, 198301.
131. I. Nakamura and Z.-G. Wang, *Soft Matter*, 2012, **8**, 9356-9367.
132. I. Gunkel and T. Thurn-Albrecht, *Macromolecules*, 2011, **45**, 283-291.
133. N. S. Wanakule, A. Panday, S. A. Mullin, E. Gann, A. Hexemer and N. P. Balsara, *Macromolecules*, 2009, **42**, 5642-5651.
134. R. Yuan, A. A. Teran, I. Gurevitch, S. A. Mullin, N. S. Wanakule and N. P. Balsara, *Macromolecules*, 2013, **46**, 914-921.
135. V. Ganesan, V. Pyramitsyn, C. Bertoni and M. Shah, *Acs Macro Letters*, 2012, **1**, 513-518.
136. L. Gwee, J.-H. Choi, K. I. Winey and Y. A. Elabd, *Polymer*, 2010, **51**, 5516-5524.
137. W.-S. Young and T. H. Epps, *Macromolecules*, 2012, **45**, 4689-4697.
138. M. J. Park and N. P. Balsara, *Macromolecules*, 2009, **43**, 292-298.
139. J. Sax and J. M. Ottino, *Poly. Eng. and Sci.*, 1983, **23**, 165-176.
140. P. W. Majewski, M. Gopinadhan and C. O. Osuji, *Soft Matter*, 2013, **9**, 7106-7116.
141. L. Ramon-Gimenez, R. Storz, J. Haberl, H. Finkelmann and A. Hoffmann, *Macromolecular Rapid Comm.*, 2012, **33**, 386-391.
142. M. J. Park and N. P. Balsara, *Macromolecules*, 2010, **43**, 292-298.
143. T. Ohtake, M. Ogasawara, K. Ito-Akita, N. Nishina, S. Ujiie, H. Ohno and T. Kato, *Chem. of Mater.*, 2000, **12**, 782-789.
144. M. J. Birnkrant, C. Y. Li, L. V. Natarajan, V. P. Tondiglia, R. L. Sutherland, P. F. Lloyd and T. J. Bunning, *Nano letters*, 2007, **7**, 3128-3133.
145. Y. Zhou, S.-k. Ahn, R. K. Lakhman, M. Gopinadhan, C. O. Osuji and R. M. Kasi, *Macromolecules*, 2011, **44**, 3924-3934.
146. M. Gopinadhan, P. W. Majewski and C. O. Osuji, *Macromolecules*, 2010, **43**, 3286-3293.
147. J. Li, K. Kamata, M. Komura, T. Yamada, H. Yoshida and T. Iyoda, *Macromolecules*, 2007, **40**, 8125-8128.
148. M. Gopinadhan, P. W. Majewski, Y. Choo and C. O. Osuji, *Physical Review Letters*, 2013, **110**, 078301.
149. M. Gopinadhan, P. W. Majewski, E. S. Beach and C. O. Osuji, *ACS Macro Letters*, 2011, **1**, 184-189.
150. H. Hu, M. Gopinadhan and C. O. Osuji, *Soft Matter*, 2014, **10**, 3867-3889.
151. D. Golodnitsky, E. Livshits, Y. Rosenberg, E. Peled, S. H. Chung, Y. Wang, S. Bajue and S. G. Greenbaum, *J. Electroanal. Chem.*, 2000, **491**, 203-210.
152. D. Golodnitsky, E. Livshits, Y. Rosenberg, I. Lapides and E. Peled, *Solid State Ionics*, 2002, **147**, 265-273.

153. D. Golodnitsky, E. Livshits and E. Peled, *Macromolecular Symposia*, 2003, **203**, 27-46.
154. D. Golodnitsky, E. Livshits, R. Kovarsky, E. Peled, S. H. Chung, S. Suarez and S. G. Greenbaum, *Electrochem. and Solid-State Lett.*, 2004, **7**, A412-A415.
155. C. M. Burba, R. Frech and B. Grady, *Electrochimica Acta*, 2007, **53**, 1548-1555.
156. L. Gitelman, M. Israeli, A. Averbuch, M. Nathan, Z. Schuss and D. Golodnitsky, *J. Comp. Phys.*, 2008, **227**, 8437-8447.
157. C. M. Burba, L. Woods, S. Y. Millar and J. Pallie, *Electrochimica Acta*, 2011, **57**, 165-171.
158. D. Golodnitsky and E. Peled, *Electrochimica Acta*, 2000, **45**, 1431-1436.
159. J. Li, J. K. Park, R. B. Moore and L. A. Madsen, *Nat. Mater.*, 2011, **10**, 507-511.
160. B. Dong, L. Gwee, D. Salas-de la Cruz, K. I. Winey and Y. A. Elabd, *Nano Letters*, 2010, **10**, 3785-3790.
161. F. Capuano, F. Croce and B. Scrosati, *J. Electrochem. Soc.*, 1991, **138**, 1918-1922.
162. W. Krawiec, L. G. Scanlon Jr, J. P. Fellner, R. A. Vaia, S. Vasudevan and E. P. Giannelis, *J. Power Sources*, 1995, **54**, 310-315.
163. W. Wieczorek, P. Lipka, G. Żukowska and H. Wyciślik, *J. Phys. Chem. B*, 1998, **102**, 6968-6974.
164. C. Capiglia, P. Mustarelli, E. Quartarone, C. Tomasi and A. Magistris, *Solid State Ionics*, 1999, **118**, 73-79.
165. F. Croce, R. Curini, A. Martinelli, L. Persi, F. Ronci, B. Scrosati and R. Caminiti, *J. Phys. Chem. B*, 1999, **103**, 10632-10638.
166. B. Kumar and L. G. Scanlon, *Solid State Ionics*, 1999, **124**, 239-254.
167. G. B. Appetecchi, F. Croce, L. Persi, F. Ronci and B. Scrosati, *Electrochimica Acta*, 2000, **45**, 1481-1490.
168. M. Marcinek, A. Bac, P. Lipka, A. Zalewska, G. Żukowska, R. Borkowska and W. Wieczorek, *J. Phys. Chem. B*, 2000, **104**, 11088-11093.
169. B. Scrosati, F. Croce and L. Persi, *J. Electrochem. Soc.*, 2000, **147**, 1718-1721.
170. F. Croce, L. Persi, B. Scrosati, F. Serraino-Fiory, E. Plichta and M. A. Hendrickson, *Electrochimica Acta*, 2001, **46**, 2457-2461.
171. P. A. R. D. Jayathilaka, M. A. K. L. Dissanayake, I. Albinsson and B. E. Mellander, *Electrochimica Acta*, 2002, **47**, 3257-3268.
172. W. Wieczorek, Z. Florjanczyk and J. R. Stevens, *Electrochimica Acta*, 1995, **40**, 2251-2258.
173. M. Siekierski, W. Wieczorek and J. Przyłuski, *Electrochimica Acta*, 1998, **43**, 1339-1342.
174. Y. W. Kim, W. Lee and B. K. Choi, *Electrochimica Acta*, 2000, **45**, 1473-1477.
175. B.-K. Choi, Y.-W. Kim and K.-H. Shin, *J. Power Sources*, 1997, **68**, 357-360.
176. A. S. Best, A. Ferry, D. R. MacFarlane and M. Forsyth, *Solid State Ionics*, 1999, **126**, 269-276.
177. V. Pryamitsyn and V. Ganesan, *Macromolecules*, 2014, **47**, 6095-6112.

178. A. S. Best, J. Adebahr, P. Jacobsson, D. R. MacFarlane and M. Forsyth, *Macromolecules*, 2001, **34**, 4549-4555.
179. P. Johansson, M. A. Ratner and D. F. Shriver, *The Journal of Physical Chemistry B*, 2001, **105**, 9016-9021.
180. J. Xie, R. G. Duan, Y. Han and J. B. Kerr, *Solid State Ionics*, 2004, **175**, 755-758.
181. L. M. Bronstein, R. L. Karlinsey, K. Ritter, C. G. Joo, B. Stein and J. W. Zwanziger, *Journal of Materials Chemistry*, 2004, **14**, 1812-1820.
182. *Electrochimica Acta*, 1998, **43**, 1135.
183. M. Popall, M. Andrei, J. Kappel, J. Kron, K. Olma and B. Olsowski, *Electrochimica Acta*, 1998, **43**, 1155-1161.
184. H.-M. Kao, T.-T. Hung and G. T. K. Fey, *Macromolecules*, 2007, **40**, 8673-8683.
185. D. Saikia, Y.-H. Chen, Y.-C. Pan, J. Fang, L.-D. Tsai, G. T. K. Fey and H.-M. Kao, *Journal of Materials Chemistry*, 2011, **21**, 10542-10551.
186. P. Barbosa, L. Rodrigues, M. Silva, M. Smith, A. Goncalves and E. Fortunato, *Journal of Materials Chemistry*, 2010, **20**, 723-730.
187. V. Di Noto, E. Negro, S. Lavina and M. Vittadello, *Polymer Electrolytes–Fundamentals and Applications, Woodhead Publishing Limited, Oxford*, 2010, 219-277.
188. V. Di Noto, S. Lavina, G. A. Giffin, E. Negro and B. Scrosati, *Electrochimica Acta*, 2011, **57**, 4-13.
189. E. Ruizhitzky and P. Aranda, *Adv. Mater.*, 1990, **2**, 545-547.
190. P. Aranda, J. C. Galvan, B. Casal and E. Ruizhitzky, *Electrochimica Acta*, 1992, **37**, 1573-1577.
191. J. C. Hutchison, R. Bissessur and D. F. Shriver, *Chem. of Mater.*, 1996, **8**, 1597-&.
192. J. L. Lutkenhaus, E. A. Olivetti, E. A. Verploegen, B. M. Cord, D. R. Sadoway and P. T. Hammond, *Langmuir*, 2007, **23**, 8515-8521.
193. D. M. Smith, C. Y. Li and T. J. Bunning, *J. P. Sci. Part B: Poly. Phys.*, 2014, **52**, 232-250.
194. T. J. Bunning, L. V. Natarajan, V. P. Tondiglia and R. L. Sutherland, *Annu. Rev. Mater. Sci.*, 2000, **30**, 83-115.
195. C. Y. Li and T. J. Bunning, *Curr. Opin. Chem. Engin.*, 2013, **2**, 63-67.
196. C. Y. Li, M. J. Birnkrant, L. V. Natarajan, V. P. Tondiglia, P. F. Lloyd, R. L. Sutherland and T. J. Bunning, *Soft Matter*, 2005, **1**, 238-242.
197. M. J. Birnkrant, H. K. McWilliams, C. Y. Li, L. V. Natarajan, V. P. Tondiglia, R. L. Sutherland, P. F. Lloyd and T. J. Bunning, *Polymer*, 2006, **47**, 8147-8154.
198. M. J. Birnkrant, C. Y. Li, L. V. Natarajan, V. P. Tondiglia, R. L. Sutherland and T. J. Bunning, *Soft Matter*, 2011, **7**, 4729-4734.
199. D. M. Smith, S. Cheng, W. D. Wang, T. J. Bunning and C. Y. Li, *J. Pow. Sour.*, 2014, **271**, 597-603.

Graphic Abstract:

We discuss recent progresses on anisotropic ion transport in solid polymer electrolytes.

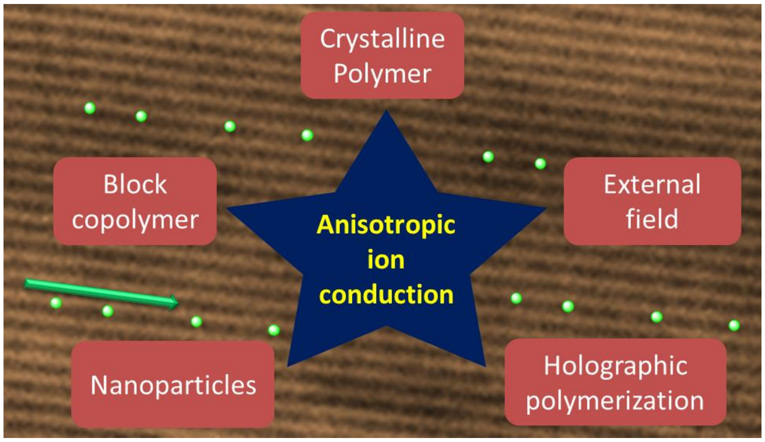

Shan Cheng completed her B.S. degree in Polymer Science and Engineering at Jilin University, Changchun, China in 2009. She recently received her Ph.D. degree in Materials Science and Engineering from Drexel University under the supervision of Dr. Christopher Li. Her research is focused on understanding the correlation between crystalline morphology and ion transport in semi-crystalline solid polymer electrolytes.

Derrick Smith received his B.S. and M.S. degrees in Material Science and Engineering from Drexel University. He is currently completing a PhD in Material Science at Drexel under the direction of Dr. Christopher Li. His research involves combining holographic polymerization and electrolyte chemistries to create nanoscaffolded polymer electrolyte membranes with enhanced mechanical properties for battery and fuel cell applications. He is an NSF-IGERT and NSF-GRFP fellow.

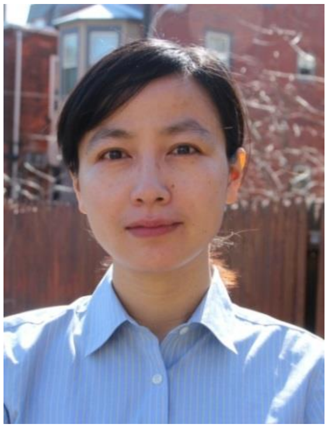

Prof. Qiwei Pan received her Ph.D. in Polymer Science from Peking University, China. She joined South China University of Technology, the Department of Materials Science and Engineering in 2008. She is currently a visiting professor at Drexel University. Her research activity is focused on the synthesis and characterization of liquid crystalline polymers and polymer electrolytes.

Dr. Shijun Wang received his Ph.D. in electrochemistry from University of Southern Mississippi. He then moved to University of Texas at Austin working with Prof. Allen Bard as a postdoc researcher. He is currently a postdoc scientist at Drexel University under the supervision of Prof. Christopher Li. His research interest is focused on solid polymer electrolytes for lithium batteries.

Christopher Li received his Ph.D. in Polymer Science from the University of Akron. He joined Drexel University, the Department of Materials Science and Engineering in 2002 as an assistant professor, and was promoted to associate and full professor in 2007, and 2011, respectively. He received an NSF Career award in 2003, an NSF Creativity Award in 2011, became a Fellow of the American Physical Society in 2012, and a Fellow of the North American Thermal Analysis Society in 2014. His research interests center on the structure and morphology of ordered polymeric systems and hybrid materials.